

Spectroscopic trace gas detection in air-based gas mixtures: Some methods and applications for breath analysis and environmental monitoring

Cite as: J. Appl. Phys. **131**, 220901 (2022); <https://doi.org/10.1063/5.0091263>

Submitted: 13 March 2022 • Accepted: 04 May 2022 • Published Online: 13 June 2022

 Jinbao Xia,  Feng Zhu, James Bounds, et al.

COLLECTIONS

Paper published as part of the special topic on [Non-Invasive and Non-Destructive Methods and Applications Part I â€” Festschrift](#)

 This paper was selected as an Editor's Pick



View Online



Export Citation



CrossMark

ARTICLES YOU MAY BE INTERESTED IN

[Micro-strains, local stresses, and coherently diffracting domain size in shock compressed Al\(100\) single crystals](#)

Journal of Applied Physics **131**, 225902 (2022); <https://doi.org/10.1063/5.0090680>

[Electrical and thermal percolation in two-phase materials: A perspective](#)

Journal of Applied Physics **131**, 230901 (2022); <https://doi.org/10.1063/5.0091291>

[Determination of the charge carrier density in organic solar cells: A tutorial](#)

Journal of Applied Physics **131**, 221101 (2022); <https://doi.org/10.1063/5.0094955>

Journal of
Applied Physics

Special Topics Open for Submissions

Learn More




Spectroscopic trace gas detection in air-based gas mixtures: Some methods and applications for breath analysis and environmental monitoring

Cite as: J. Appl. Phys. **131**, 220901 (2022); doi: [10.1063/5.0091263](https://doi.org/10.1063/5.0091263)

Submitted: 13 March 2022 · Accepted: 4 May 2022 ·

Published Online: 13 June 2022



Jinbao Xia,^{1,2,3}  Feng Zhu,⁴  James Bounds,³ Eshtar Aluauee,³ Alexandre Kolomenskii,^{3,a)} 
Qian Dong,^{5,a)}  Jingliang He,¹ Cain Meadows,³ Sasa Zhang,⁶ and Hans Schuessler³ 

AFFILIATIONS

¹State Key Laboratory of Crystal Materials, Shandong University, Jinan 250100, China

²State Key Laboratory of Applied Optics, Changchun Institute of Optics, Fine Mechanics and Physics, Chinese Academy of Sciences, Changchun 130033, China

³Department of Physics and Astronomy, Texas A&M University, College Station, Texas 77843-4242, USA

⁴School of Physics and Astronomy, Sun Yat-sen University, Zhuhai, Guangdong 519082, China

⁵Department of Computer Science, Jinan University, Guangzhou 510632, China

⁶School of Information Science and Engineering, Shandong University, Jinan 250100, China

Note: This paper is part of the Special Topic on Non-Invasive and Non-Destructive Methods and Applications Part I: Festschrift.

a) Authors to whom correspondence should be addressed: alexandre-kolomenski@tamu.edu and dongq8@jnu.edu.cn

ABSTRACT

Laser absorption spectroscopy as a powerful tool for detecting trace gases has been widely used in the monitoring of atmospheric greenhouse gases, pollutions, and respiration processes, including human breath analysis. The detection is based on the light absorption when it propagates through a medium. Most inorganic and organic molecules have characteristic absorption lines in the mid-infrared (mid-IR), which correspond to fundamental vibrational modes and in the near-IR (first overtones) presenting their absorption fingerprints. Here, we summarize the recent developments of the three techniques, namely, wavelength modulation spectroscopy (WMS), cavity ring-down spectroscopy (CRDS), and frequency comb spectroscopy (FCS), and describe their main features as well as possible applications, illustrated by recent experimental results. Emphasis is made on methane detection as applied to breath analysis and atmospheric monitoring. For the WMS technique, we consider local measurements with a multipass cell and also kilometer long open-path configurations for the near-IR and mid-IR spectral regions. The results of measurements of methane in exhaled breath with the CRDS technique in the near-IR are presented for a group of subjects of different ages. We consider various schemes of the FCS that enable fast broadband detection, including direct spectroscopy, dual FCS, and Vernier FCS, and review numerous applications of this approach that revolutionized the field of absorption spectroscopy. The current trends and possible future developments and applications are also discussed.

Published under an exclusive license by AIP Publishing. <https://doi.org/10.1063/5.0091263>

I. INTRODUCTION

Laser absorption spectroscopy (LAS) as a powerful tool to detect trace gases was widely used in atmospheric environment monitoring and studies of air-related phenomena, such as anthropogenic processes and the greenhouse effect, atmospheric chemical reactions, respiration of flora and fauna, and combustion processes. The basic principle of LAS relies on the Beer–Lambert law. When

the light propagates through a medium, it is absorbed due to transitions from lower to higher energy levels of the atomic or molecular system. Most inorganic (oxygen, nitric oxide, hydrogen sulfide, etc.) and organic molecules (methane, acetylene, etc.) have characteristic absorption lines in the mid-infrared (mid-IR) spectral region, corresponding to fundamental vibrational modes of molecules and in the near-IR region, where molecular first overtones are located, although with much smaller optical absorption cross sections. From these

characteristic absorption molecular lines, presenting spectral fingerprints, the molecules can be uniquely identified. The laser spectroscopy detection of gases also provides a fast and real-time means for online monitoring. In atmospheric monitoring, researchers use laser spectroscopy to detect trace gases to understand the status, origin, and evolution of atmospheric pollution. As such, the concentrations of ammonia¹ and carbon monoxide² were measured. In breath analysis, some volatile organic compounds (VOCs) have been established as biomarkers. Measuring their concentrations in exhaled breath aids in disease diagnosis.³ For example, a laser spectroscopic system can be used for the detection of acetone in breath, which correlates with an abnormal metabolic status, indicative of diabetes.⁴ Compared to other methods, such as gas chromatography with mass spectroscopy, the LAS approach can substantially reduce the analysis time, employs less expensive and bulky equipment, and simplifies or does not require any sample preparation at all. Another technique, labeled electronic nose, is so far in its infancy and needs further development before it can compete in terms of sensitivity and specificity, especially when several compounds should be detected. In this paper, we will describe several LAS techniques, including wavelength modulation spectroscopy (WMS),^{5,6} cavity ringdown spectroscopy (CRDS), and frequency comb spectroscopy (FCS). The progress in the LAS field critically depends on the development of new laser sources and detectors, which are employed in all these methods. Recent advances in the generation and detection of infrared radiation⁷ have a considerable impact on the development of sensitive detection methods of gases. Many exciting new opportunities came about with the development of frequency comb laser sources,⁸ enabling fast capturing of broadband spectra without the need for scanning the optical wavelength. Of course, this paper provides only a partial overview of the field. In recent years, a variety of sensitive spectroscopic techniques were developed, in particular, the progress in photoacoustic spectroscopy (PAS),^{9,10} quartz-enhanced PAS,^{11,12} and integrated cavity output spectroscopy (ICOS)¹³ was described in recent reviews. Applications to combustion diagnostics¹⁴ and stand-off chemical detection¹⁵ were also reviewed.

The WMS with the typical detection limit from ppm to ppb level is relatively easier to implement compared to the CRDS and the FCS techniques. For cavity ringdown spectroscopy, the complexity and cost of a typical system is higher, while the detection limit can be improved from ppb to ppt level. Although the FCS detection limit is roughly similar to the WMS, it has several advantages, including possibilities of fast and multispecies detection. In addition, combining the FCS with a multipass or resonant cavity provides both the possibility of a local measurement and a long interaction path allowing us to achieve high sensitivity in the ppb range.

In this paper, we summarize the recent developments of the three mentioned techniques and describe their features, as well as possible applications, illustrated by recent experimental results obtained in the group of Schuessler and Kolomenskii at Texas A&M University in collaboration with the groups of Zhang and He (Shandong University) and Zhu (Sun Yat-sen University).

II. WAVELENGTH MODULATION SPECTROSCOPY

The WMS as a highly sensitive and relatively simple technique was widely used in atmospheric monitoring, breath analysis, and for locking the laser frequency to a specific molecular transition frequency. Its basic principle is as follows. The laser radiation from a diode laser is pumped by the injection current modulated simultaneously with a low frequency oscillation of triangular shape and high amplitude (for scanning of the optical wavelength) and a high-frequency sine-wave oscillation (for high-frequency modulation of the optical wavelength). This radiation is transmitted through an absorbing medium, gas or liquid, and the detected signal is then processed by a lock-in amplifier, so that the demodulated harmonic signal reflects the unknown concentration. We assume that the incident laser intensity and frequency are modulated as described by the following equations:

$$I(t) = \bar{I} + \Delta I \cos(\omega t), \quad (1)$$

$$\nu(t) = \bar{\nu} + \Delta\nu \cos(\omega t + \psi). \quad (2)$$

Here, \bar{I} is the average laser intensity, ΔI is the modulation amplitude, $\omega = 2\pi f$, where f is the modulation frequency, $\bar{\nu}$ is the running average of the scanning laser frequency, $\Delta\nu$ is the frequency modulation amplitude, and ψ is the phase shift between the frequency and intensity modulation. The harmonics retrieved with a lock-in amplifier can be expressed through the components $H_k(k = 1, 2, 3, \dots)$ of the Fourier series expansion,⁶

$$H_k(\bar{\nu}, \Delta\nu) = -\frac{P\chi LS}{2\pi} \int_{-\pi}^{\pi} \varphi(\bar{\nu} + \Delta\nu \cos\theta) \cos(k\theta) d\theta, \quad (3)$$

where $\theta = \omega t$, S and φ are the spectral line strength, mainly dependent on the gas temperature T , and the line shape function, respectively, P is the pressure of the gas mixture, χ is the mole fraction of the absorbing species, and L is the effective optical path length.

A WMS setup is generally composed of the following main parts (Fig. 1): a modulated laser source, a multipass absorption cell (or an optical system for sending and receiving the laser beam over

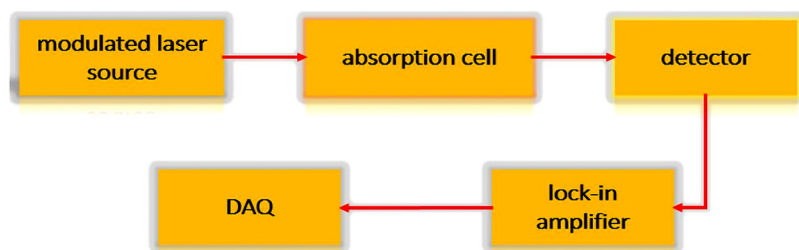


FIG. 1. Schematic of a WMS sensor.

a long open-path), a detector, a lock-in amplifier, as well as a data acquisition and processing unit (including possible digital filtering as described in the following).

Most efforts so far were directed at improving the performance of sensors by upgrading the mentioned main parts. For the laser source, as a core part of the WMS instrument, a distributed feedback (DFB) laser, an interband cascade laser (ICL), a quantum cascade laser (QCL), a vertical-cavity surface-emitting laser (VCSEL), and a difference frequency generation (DFG) source were commonly used. The employed multipass cells were mostly of Herriot¹⁶ or White¹⁷ types achieving the interaction length of tens of meters. Some novel cells, such as a mini-multi-pass cell¹⁸ and a specially designed record-breaking confocal cell¹⁹ with the effective path of hundreds of meters, also emerged in recent years. The compactness and robustness of the lock-in detection were realized with digital lock-in amplifiers implemented via digital signal processing (DSP) or using a field-programmable gate array (FPGA),²⁰ which replaced bulky stand-alone commercial lock-in amplifiers, while still preserving competitive performance. Often, various filtering algorithms were applied in signal processing to improve the signal-to-noise ratio. Overall, being relatively simple and cost-efficient, the WMS approach shows high potential in many application fields.

A. Laboratory studies for local detection

Various WMS sensors were implemented for detecting H_2O ,²¹ H_2S ,²² NH_3 ,²³ N_2O ,²⁴ and CH_4 .^{25,26} In terms of cost and performance, the sensors in the near-IR and mid-IR are quite different. Generally, the absorption cross sections of molecules in the mid-IR are larger by about two orders of magnitude compared to those in the near-IR; thus, a sensor in mid-IR potentially has a higher sensitivity. However, the components in the mid-IR, such as laser sources and detectors, are generally more expensive. Therefore, the sensor detection limit, cost, and sensor performance need to be taken into account for the sensor design. We present sensors for different trace gases in Table I, indicating laser wavelength, cell length, and the achieved detection limit. To illustrate the typical sensor design, we describe below sensors for methane and acetone, which are two important target gases in environmental monitoring and breath analysis, respectively. Xia *et al.*²⁷ reported an ultra-sensitive sensor for methane, which we show schematically in Fig. 2. For this sensor, a confocal multipass cell (MPC) with an effective interaction length of 580 m was developed. The performance of the sensor was evaluated in a series of measurements with two spectroscopic methods, namely, direct absorption spectroscopy (DAS) and WMS. Different digital filtering algorithms were implemented to improve the signal-to-noise ratio in the DAS operation mode. The WMS sensor showed a better performance with the detection limit of 560 ppt achieved at 290 s integration time.

To measure fugitive methane emissions, a portable sensor with both high sensitivity and fast response time was developed recently by Oliaee *et al.*²⁸ with a continuous-wave thermoelectrically cooled GaSb-based distributed feedback diode laser emitting at a wavelength of $3.27\ \mu\text{m}$ (Fig. 3.). The effective optical path length of the multipass cell used in the sensor was 6.8 m. The sensor was evaluated with the DAS and WMS techniques. Under

TABLE I. Spectroscopic (WMS) sensors used for detection of various trace gases.

Gases	Laser wavelength	Optical path	Detection limit	Reference
Methane	7503 nm	76 m	40 ppb	42
	1653 nm	10 cm	5.8 ppm	43
	1653 nm	290 m	1.2 ppb	25
	1653 nm	100 cm	0.1 ppm	44
	1654 nm	145 cm	130 ppb	45
	1653 nm	20 m	90 ppb	46
	$3.3\ \mu\text{m}$	58 m	1.4 ppb	47
	$3.3\ \mu\text{m}$	1.3 m	0.505 ppm	48
	1653 nm	26.4 m	79 ppb	49
	$2.3\ \mu\text{m}$	10 cm	2 ppm	50
Carbon monoxide	$2.3\ \mu\text{m}$	14.5 m	6 ppb	51
	$2.3\ \mu\text{m}$	2 m	1.29 ppm	52
	$4.69\ \mu\text{m}$	399 cm	9 ppb	53
	1578 nm	55.1 m	0.29 ppm	54
	$4.6\ \mu\text{m}$	76 m	0.5 ppb	55
Ammonia	1512 nm	100 cm	26 ppbv	56
	9.56	5 m	63.2 ppb	57
	$10.39\ \mu\text{m}$	179 cm	2.8 ppm	58
	1531 nm	30 m	53 ppb	59
	1530 nm	40 cm	0.12 ppm	60
Acetylene	1.53 μm	21.9 m	76.75 ppb	61
	1530 nm	10 m	14.3 ppb	62
	1530 nm	52.2 m	0.2 ppm	44
	1553 nm	30 cm	0.54 ppm	63
	2004 nm	27.5 m	68 ppm	64
Carbon dioxide	2004 nm	12 m	10 ppm	65
	$4.319\ \mu\text{m}$	1 cm	$\sim 0.3\%$	66
	$4.319\ \mu\text{m}$	29.8 m	0.72 ppb	67
	1572 nm	16 m	2.7 ppb	68
	1579 nm	20 m	769 ppm	69
Nitrogen oxide	5.26 μm	100 m	124 ppt	70
	$5.3\ \mu\text{m}$	3 m	0.1 ppm	71
	$5.26\ \mu\text{m}$	310 mm	unknown	72
Formaldehyde	$3.43\ \mu\text{m}$	100 m	1.6 ppb	73
	$3.59\ \mu\text{m}$	3.75 m	1.5 ppb	74
	$3.59\ \mu\text{m}$	50 m	0.58 ppb	75

the WMS operation, the detection limit was better than 1 ppb at the integration time of 1 s.

The interest in detection of acetone as a biomarker for breath analysis and diagnostics has stimulated the development of several sensors. The acetone molecule has four strong fundamental absorption bands in the mid-IR: 3–4, 5.5–6, 7–7.5, and 8–8.5 μm , and different research groups developed acetone sensors in these wavelength intervals. Schwarm *et al.*²⁹ developed a calibration-free acetone sensor for detection in exhaled breath with the interference correction method based on the WMS near 8.2 μm achieving the detection limit of 0.11 ppm. Nadeem *et al.*³⁰ reported the acetone sensor employing WMS and a single-mode widely tunable ($\sim 300\ \text{cm}^{-1}$) external-cavity quantum cascade laser operating around 8 μm . In this sensor, the compact multipass cell was used

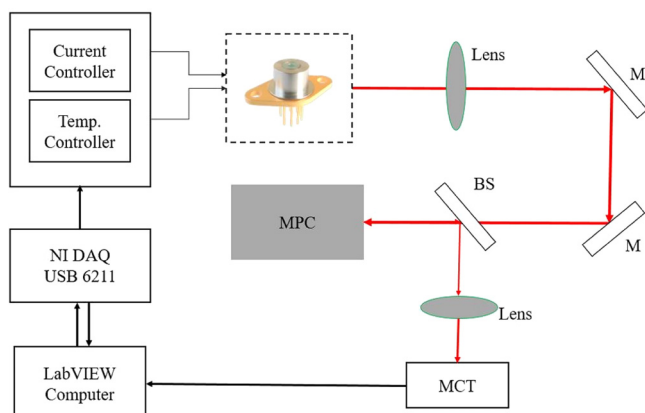


FIG. 2. The layout of the methane sensor. ICL laser with a wavelength of $3.2\ \mu\text{m}$ was coupled to a multipass cell (MPC); after 579 reflections, the laser beam exited the MPC and was focused on a Vigo MCT detector. The whole sensor was controlled by a LabVIEW program, which performed laser modulation, signal demodulation, signal analysis, and displaying.

to improve the detection limit to 15 ppbv with an integration time of 10 s, which yielded the noise-equivalent absorption (NEA) sensitivity of $1.9 \times 10^{-8}\ \text{cm}^{-1}\ \text{Hz}^{-1/2}$. Xia *et al.*³¹ carried out acetone measurements at a laser wavelength near $3\ \mu\text{m}$ using a Herriot cell with an effective optical path of 24 m and achieved the detection limit of 0.58 ppm in 1 s. We have depicted the schematic diagram of such a sensor in Fig. 4(a). A mid-IR frequency comb was used to characterize the DFB-ICL emission line by observing the beating signal between the two lasers. Due to the choice of the absorption lines, the influence of water and CO_2 was minimized. The Allan deviation analysis of the sensor showed that the sensor detection limit was about ~ 0.12 ppm with the integration time of 60 s [Fig. 4(b)].

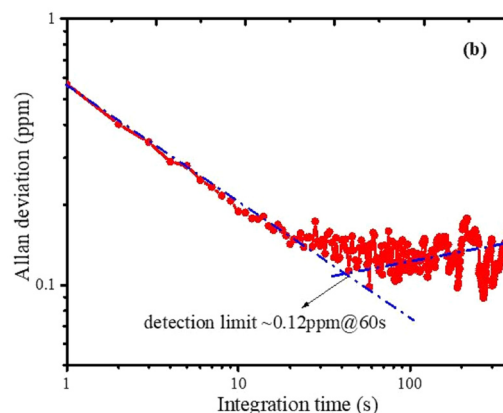
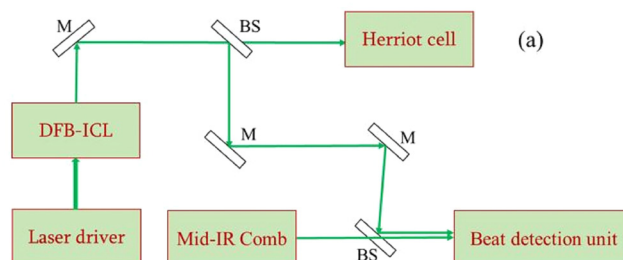


FIG. 4. (a) Schematic of the acetone WMS sensor in the mid-IR. The ICL-DFB laser beam with the center wavelength of $3.367\ \mu\text{m}$ was split into two beams: one was coupled to a Herriot cell with the effective length of 24 m for acetone measurement and the other was used for detection of the beat-signal with a mid-IR comb to retrieve the laser linewidth. (b) The Allan deviation of the sensor vs time, showing that the sensor detection limit was about ~ 0.12 ppm with the integration time of 60 s. Adapted with permission from Xia *et al.*, OSA Contin. 2, 640 (2019). Copyright 2019 The Optical Society.

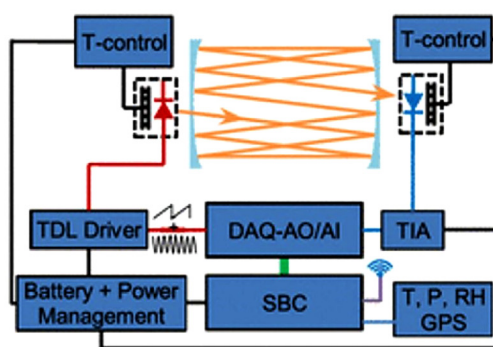
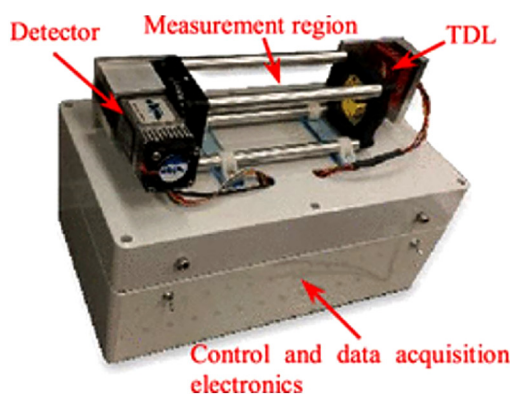


FIG. 3. A view of the compact methane sensor and its schematic. A GaSb-based DFB laser emitting at $3.27\ \mu\text{m}$ was coupled to a multipass cell with an effective length of 6.8 m. After many passes, the transmitted beam is detected by a TE-cooled photovoltaic MCT photodetector and demodulated by a software-based lock-in amplifier. Reproduced with permission from Oliaee *et al.*, ACS Sensors 7, 564 (2022). Copyright 2022 American Chemical Society.

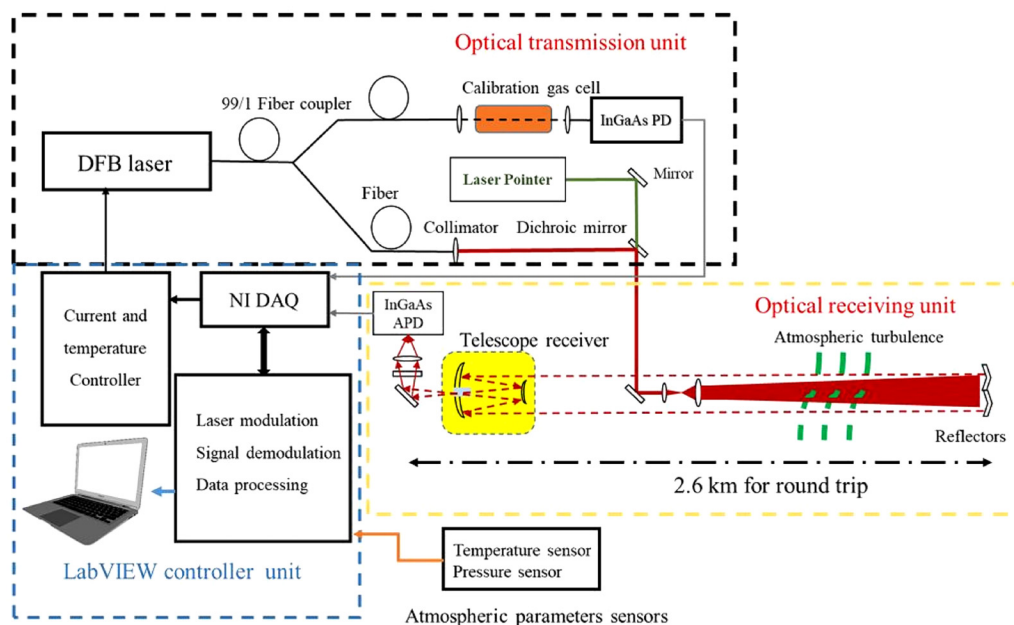


FIG. 5. Schematic of the open long-path remote sensing system. A $1.65\ \mu\text{m}$ DFB laser beam was split and used in two channels: one for system calibration by measuring the calibration gas and another for the long-path measurement with aligning by a green laser pointer. The reflected signal was collected by a telescope and focused on an InGaAs avalanche photodiode. The detected signal was demodulated by a digital lock-in amplifier based on a LabVIEW code, and the latter also implemented the current modulation of the DFB laser. Pressure and temperature sensors monitored the parameters of the atmosphere. Reproduced with permission from Xia *et al.* Opt. Lasers Eng. 117, 21 (2019). Copyright 2019 Elsevier.

Overall, the WMS-based sensitive detection of acetone is a feasible and practical approach.

B. Remote long-path WMS sensing

WMS was also used in the long-path sensing of trace gases, such as methane, carbon dioxide, etc. Michel *et al.*³² used a quantum cascade laser at $\sim 8\ \mu\text{m}$ with a power of 40 mW to monitor methane over a 458 m path with the detection limit of 10 ppb at a 1 Hz acquisition rate. In this system, an in-line N_2O gas cell was used for system stabilization. The sensor endured quite well harsh environmental conditions, including snow, rain, wind, and changing temperatures.

Xia *et al.* developed an open-path remote sensing optical system with a near-IR laser source operating close to two wavelengths of ~ 1654 and ~ 1602 nm for measuring methane and carbon dioxide, respectively.³³ The schematic of the system is shown in Fig. 5. The in-line gas cell with a calibrated methane or carbon dioxide gas of 1% and 100% concentrations, respectively, was utilized in the reference channel to retrieve in real time the actual gas concentration from comparison with the signal channel. The sensor was evaluated first indoor, and then it was set up on an airport runway with a 2.6 km round trip path to measure the path-averaged concentration of methane for more than 10 h. The detection limit of the sensor for methane determined by the Allan deviation analysis of the data was 20 ppb.

The system was designed for the detection of methane over a kilometer long distance with only 10 mW of the optical power from the laser source. In such a long-distance experiment, two key factors should be considered to get better performance. First, the laser scanning and modulation frequencies should be optimized. The transmission signal within the frequency interval of the atmospheric turbulence is strongly suppressed, which can be seen from the calculated by Fourier transform power spectral density of the signal. Therefore, by modulating the wavelength above the cut-off frequency the influence of random variations due to turbulence can be effectively reduced. In our case, the scanning frequency was set to 100 Hz and the modulation frequency was set to be 25 kHz. The second point is that the influence of the signal power fluctuations caused by the laser itself should be minimized as much as possible. Thus, a 1f signal was also demodulated and used for the normalization of the 2f-signal to decrease the effect of the laser power fluctuations. For the data processing, the distance between the telescope and the retroreflector needs to be measured independently to be a known parameter. With the laser power enhanced by a fiber amplifier, even longer detection distances can be reached. A combination of multiple laser sources can increase the bandwidth for the detection of multiple trace gases, which for remote sensing can be a feasible alternative to a more cost and power consuming frequency comb spectroscopy.³⁴

Zhang *et al.* developed an open-path gas sensor adopting a QCL as a laser source with the center wavenumber at $2203.73\ \text{cm}^{-1}$

for the detection of atmospheric N_2O .³⁵ In this sensor, the 1f-normalization of the WMS signal was also employed to suppress the influence of the laser power fluctuations. A 20 ppm N_2O standard gas was used for calibration. With the Allan deviation analysis, the detection limit for the sensor was determined to be 1.1 and 0.14 ppb with the integration times of 1 and 95 s, respectively. In the mentioned works, the distance between the receiver and the reflector had to be accurately measured with a rangefinder or other instrument. Yang *et al.* developed the phase retrieval approach of the first harmonic signal (1f phase) in the WMS technique to measure the gas concentration and the path length simultaneously.³⁶ This approach has been experimentally validated by measuring CO_2 concentration in the open-path configuration. The sensor was evaluated by a long-path (over 700 m) 7-day continuous measurement. The detection limit of about 2 ppm with an averaging time of one second was achieved.

We note that for remote sensing of gas concentrations, a continuous wave integrated path differential absorption (IPDA) LIDAR can be used, which however, unlike WMS, uses intensity modulation. Such a system employs two lasers with the wavelength of the first (online) laser at the center of the absorption line and the wavelength of the second (offline) laser selected to be outside of the absorption line. The concept of the CW system³⁷ designed for CO_2 IPDA measurements is as follows. The online and offline seed laser radiations with spectral properties chosen for CO_2 detection are intensity modulated (each at its own frequency) and combined using fiber coupler and then are simultaneously amplified to increase the transmitted power by a single erbium doped fiber amplifier (EDFA). A small fraction of power inside of the EDFA is sent to a reference detector for power normalization. The backscattered signals of the lasers from the target surface are collected with a telescope, optically filtered with a narrow band optical filter, and detected by a single detector. Both channels are amplified, electronically filtered, and then digitized to retrieve the CO_2 column with the detection limit of better than 0.3 ppm. We note that the WMS technique can also be used in such LIDAR systems.

C. Methods of data filtering and processing

To get a better signal-to-noise ratio, some novel digital filtering algorithms were implemented for data processing, such as Kalman filtering, wavelet filtering, and neural network algorithms.^{38–41} Zheng *et al.*³⁸ developed a wavelet-denoising method to suppress the noise in the 2f-signal of methane sensor at $1.654\text{ }\mu\text{m}$. With wavelet-denoising method, the minimum detection limit was reduced from 4 to 1 ppm.

Xia *et al.*³⁹ used the Kalman filter technique to improve the open-path sensor performance. Zhu *et al.*⁴⁰ used an improved Savitzky–Golay filtering algorithm to denoise online measurement of an oxygen content in a pharmaceutical vial. This method can match the efficacy of the wavelet analysis and is even faster with a 300 ms response time, showing that it was suitable for online measurement of the gas concentration. Tian *et al.*⁴¹ used a trained on an extensive data set neural network algorithm to denoise the signal. In terms of algorithm complexity, the Kalman filter is a simpler choice for real time online monitoring, which is also suitable to be implemented in a microcontroller unit or with other data processing approaches.

In summary, the advantages of WMS that was realized in various sensors (see Table I) are as follows: (1) It can be adapted to a desired detection sensitivity range since detection limits from ppm to ppt were reported. (2) It is relatively easy to implement and has been commercialized for some trace gases avoiding the strict requirements for optimal optical alignment as compared to cavity ringdown spectroscopy. (3) WMS technique has wide range of applications and has been used in combustion studies, lidar systems to retrieve the temperature, pressure, etc. WMS has also some disadvantages compared to other techniques. Due to commonly narrow tunability of the laser wavelength, a single laser source often can detect only one species. The simultaneous detection of several species requires a combination of lasers with the required wavelength intervals. Thus, for a multi-component gas analysis, a combination of sensors working in different spectral intervals (like near-IR and mid-IR) is a possible direction for future work. Reaching the high sensitivity in the range of ppt can require the increase of the multipass cell length resulting in the sensor becoming heavy and bulky. Consequently, the development of a compact, robust, and sensitive sensor is currently another research direction.

III. CAVITY RINGDOWN SPECTROSCOPY IN THE NEAR-IR REGION FOR ANALYSIS OF EXHALED BREATH

The near-IR continuous-wave cavity ringdown spectroscopy (CW-CRDS) technique is applied to determine methane concentration in human breath samples. Methane is the biomarker indicative of colon and digestive problems. A narrow-linewidth distributed feedback (DFB) diode laser was used to achieve sensitive detection with a high-finesse cavity by employing high reflectivity mirrors. The laser output wavelength is tuned across the absorption line peaks in the near-IR region by adjusting the temperature and current of the DFB diode laser. The experimental setup has a 172 cm long cavity and a decay time of $\sim 420\text{ }\mu\text{s}$ for the empty cavity corresponding to a path of $\sim 132\text{ km}$. The experimentally measured absorbance spectra are fitted with spectroscopic data from the HITRAN database.⁷⁶ CH_4 concentrations were measured for an exhaled breath of 22 volunteers with different health conditions.

A. Development and characteristics of the CRDS technique

Cavity ringdown spectroscopy (CRDS) is a sensitive technique that can directly measure small absorbance and allows inferring the absorber concentration. CRDS has high sensitivity; however, it requires a precise alignment since otherwise higher order modes are excited that preclude accurate measurements.⁷⁷

The basic concept of the CRDS technique involves the utilization of a high-finesse cavity with high reflectivity mirrors. The laser light is transmitted into a resonator and reflects back and forth, causing intensity build-up at resonant conditions. After reaching high intensity, the laser radiation is turned off with an acousto-optic modulator (AOM), which results in intensity temporal decay. This decay is measured as the ringdown signal on a photodetector. The ringdown time is registered for each wavelength, which is

changed in small increments through the wavelength range corresponding to the absorption peaks of interest.

The idea of the CRDS appeared in the early 1980s. CRDS was developed to measure the reflectivity of highly reflective mirrors in an optical cavity.⁷⁸ Romanini *et al.* in 1997 demonstrated CRDS employing a tunable CW single frequency laser source and achieved the detection limit of 10^{-9} cm^{-1} or 5×10^{-8} per pass through the sample.⁷⁹ Their experimental setup was similar to that of Anderson *et al.*⁷⁸ except that they used an AOM. Gatti *et al.* in 2015 introduced a comb-locked cavity ringdown spectrometer in the near-IR from 1.5 to $1.6 \mu\text{m}$ with a high-finesse passive cavity containing a gas sample by employing flat mirrors of 99.9975% reflectivity and achieved the detection limit of $5.7 \times 10^{-12} \text{ cm}^{-1}$ over a 75 s long spectral acquisition of a single absorption feature.⁸⁰ In 2016, McHale *et al.*⁸¹ used open-path CRDS with mirror reflectivity of better than 99.996% for methane measurements in ambient air at a wavelength of 1742 nm. The fast development of CRDS stimulated its employment in many applications. CRDS was utilized in analytical and atmospheric chemistry, medical and biological applications, etc., in particular, for analysis of exhaled breath.⁸² As a diagnostic tool, the measurement of breath can provide specific information on the health status of the subject; it is non-invasive, fast, intact, and undemanding for a patient.^{77,83}

The exhaled breath contains different compounds, and the major components (with typical concentration values indicated for the end phase of exhaling) include nitrogen (78%), oxygen (13%–16%), carbon dioxide (4%–5%), inert gases (~0.9%), and water vapor (5%–6%). In addition, it contains inorganic trace gases, such as nitric oxide (10–50 ppb), nitrous oxide (1–20 ppb), ammonia (0.5–2 ppm), carbon monoxide (0–6 ppm), and hydrogen sulfide (0–1.3 ppm), and organic VOCs, such as methane (2–10 ppm), acetone (0.3–1 ppm), ethanol, isoprene (~100 ppb), ethane (0–10 ppb), etc.⁸³

Here, we consider measurements of methane in exhaled breath with CRDS. Methane is a natural bioproduct that can be detected in the expired air. Methanogenic bacteria found in the colon can produce methane in anaerobic conditions. Methane is normally seen in human breath at concentrations near 2 ppm (close to the atmospheric concentration); however, its excessive production during metabolism and some abnormal conditions can lead to much higher concentrations.^{84,85} Obesity, irritable bowel syndrome, inflammatory bowel illnesses, anorexia, and other ailments are correlated with abnormal methane production.^{86,87} Here, after considering the theoretical background of CRDS and its experimental arrangement, we present our results on methane measurements in the breath of volunteers of different ages and health conditions.

B. Theoretical background of CRDS

The transmitted intensity (I_t) of the laser is given by the equation⁸⁸

$$I_t = I_0 \exp(-\alpha L), \quad (4)$$

where I_0 is the incident intensity of light; for a single absorbing species, the absorption coefficient $\alpha = \sigma n$, σ is the absorption

cross section of the species at a particular wavelength, L is the path length of the radiation interaction with the sample, and n is the number density of the absorbing molecules.

In the case of an empty cavity, the main losses are due to reflections and diffraction. Ignoring the effects of the diffraction, the intensity of light in an empty cavity after interruption of the laser source will decay exponentially according to the expression

$$I(t) = I_0 \exp\left[-(1-R)\frac{tc_0}{L}\right]. \quad (5)$$

The transmitted intensity of laser light for an empty cavity can be written as $I(t) = I_0 \exp(-t/\tau_0)$ with the rate determined by the cavity ringdown time,

$$\tau_0 = \frac{t_r}{2(1-R)}, \quad (6)$$

where $t_r = 2L/c_0$ is the travel time for a round trip and c_0 is the speed of light in the empty cavity. With a gaseous sample inside the cavity, the molecules of the sample absorb the laser beam that is injected into the cavity, so the intensity decays faster due to the absorption loss,

$$I(t) = I_0 \exp\left[-(1-R+\alpha L)\frac{tc}{L}\right], \quad (7)$$

where c is the speed of light in the cavity filled with the gas. The ringdown time (decay time constant) in this case is given by

$$\tau_1 = \frac{t_r}{2[(1-R)+\alpha L]}. \quad (8)$$

The absorption coefficient at a given wavelength can be evaluated from the known ringdown time in the empty cavity and the one for the cavity filled with the absorbing species, and assuming $c = c_0$, we obtain

$$\alpha = \frac{1}{c} \left(\frac{1}{\tau_1} - \frac{1}{\tau_0} \right), \quad (9)$$

with τ_0 and τ_1 determined by Eqs. (6) and (8), respectively.

For the determination of concentrations of N_s constituent components of a gas mixture, we equate for each measured wavelength experimentally determined absorption coefficients to the sum of the simulated contributions of the components to the absorption,

$$\alpha_{\text{exp}}(\lambda) = \sum_{l=1}^{N_s} \alpha_{\text{sim},l}(\lambda) = \sum_{l=1}^{N_s} n_l \sigma_l(\lambda), \quad (10)$$

where n_l are the molecular densities and σ_l are known absorption cross sections of the gas components that are determined from a database, such as HITRAN.⁷⁶ Using the formulas $n_l = PC_l/(k_B T)$, where P is the pressure of the gaseous sample and $C_l = n_l/n$ are unknown fractional concentrations, Eq. (10) can be presented in

the form

$$\sum_{l=1}^{N_s} A_{ml} C_l = B_m \text{ with } A_{ml} = \sigma_l(T, P, \lambda_m) \text{ and } B_m = \frac{1}{c n} \left(\frac{1}{\tau(\lambda_m)} - \frac{1}{\tau_0(\lambda_m)} \right), \quad (11)$$

where n is the overall molecular density of the gas sample and T and P are the gas temperature and pressure. Here, we introduced the vector $\vec{B} = \{B_1, \dots, B_N\}$ that is determined by the results of measurements at N wavelengths λ_m ($m = 1, \dots, N$) and the matrix A with elements A_{ml} ($m = 1, \dots, N$ and $l = 1, \dots, N_s$) that is calculated from the spectral database. Provided that the number of measurements N is larger than the number of species N_s , the vector of unknown concentrations $\vec{C} = \{C_1, \dots, C_{N_s}\}$ that gives the least squares deviation of the left and right parts of Eq. (11) can be determined as⁸⁹

$$\vec{C} = (A^T A)^{-1} A^T \vec{B}, \quad (12)$$

where A^T is the transpose of matrix A .

C. Experimental setup

The schematic of our CRDS setup is shown in Fig. 6. The measurements were performed at 70 Torr by utilizing a DFB laser

at 1653 nm and a 172 cm long cavity with 99.9987% high reflectivity mirrors (Layertec, GmbH). The calculated finesse of the cavity is $F = \pi\sqrt{R}/(1-R) \approx 242\,000$.⁹⁰ A He-Ne laser was used for the system alignment.

The beam deflected with the acousto-optic modulator (AOM) is sent to the cavity, so the AOM can work as a fast-optical switch to turn the beam on and off. A piezoelectric transducer (PZT) is actuated by a triangular shape voltage and is connected to the concave mirror of the cavity, thus modulating the cavity mode frequencies. When the resonance frequency of the cavity mode is matched with the laser frequency, high intensity inside the cavity builds up. After the incident beam is shut off, the decaying signal on an InGaAs photodetector is registered. The signal from the photodetector is sent to the FPGA device, which enables the recording of the ringdown time as the measurement progresses and the wavelength is changing. A Python software code allows the user to set the temperature and the laser current and enables scanning over the desired wavelength range.

D. Results on methane measurements in exhaled breath

In general, the exhaled breath samples contain significant amounts of carbon dioxide and water, as can be seen in Fig. 7, which depicts the ringdown time vs wavelength clearly showing the absorption transmission dips of $^{12}\text{CH}_4$, $^{13}\text{CH}_4$, CO_2 , and H_2O in measured

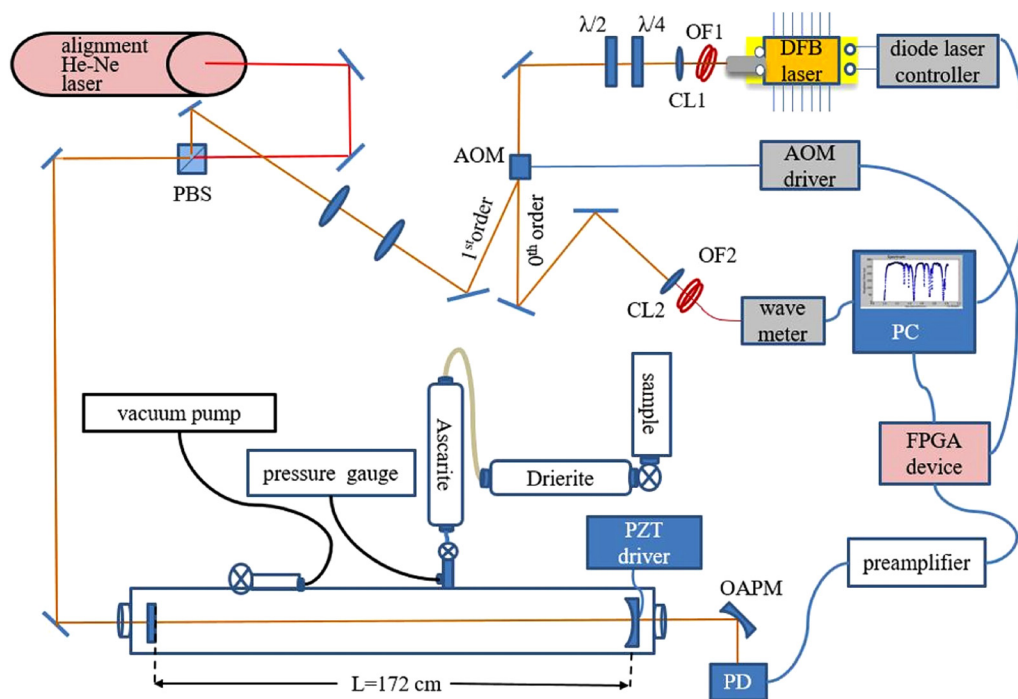


FIG. 6. Schematic diagram of the experimental setup. The first order diffraction of the laser beam is directed to the optical cavity, while zeroth order beam is used for monitoring the wavelength. A He-Ne laser was used for the system alignment. Drierite and Ascarite are optionally used for filtering out H_2O and CO_2 when they interfere with the measurement. OF1 and OF2 are optical fibers, CL1 is a collimating lens and CL2 is a coupling lens, OAPM is an off-axis parabolic mirror, and PZT driver actuates a piezoelectric transducer to scan the cavity length.

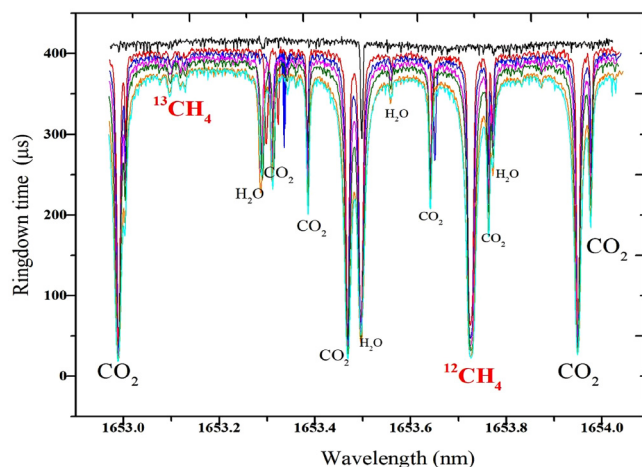


FIG. 7. Ringdown time vs wavelength measured for exhaled breath of one of the subjects at different pressures; from top to bottom, different colors represent: 0 (black, empty cavity), 20 (red), 30 (blue), 40 (magenta), 50 (green), 70 (orange), and 80 Torr (mint).

at different pressures exhaled breath samples. These measurements were done without filters containing Drierite and Ascarite that can be used to reduce the content of CO_2 , and H_2O , and the sufficiently high spectral resolution allowed us to clearly observe different absorption peaks without their overlap. As Fig. 7 shows, at low pressure, the signals are small. However, achieving higher pressure requires larger samples and leads to the broadening of the spectral lines. Considering both factors, 70 Torr was chosen as the optimal pressure. The total scan time was 1 h and 20 min per 1000 data points.

After the full scan in the range (1652.75–1654.25 nm), the data are fitted using HITRAN database⁷⁶ with a Python script. The concentration of each type of molecule is determined by the procedure presented by Eqs. (11) and (12).

Figure 8(a) reports the absorption peaks and concentrations of $^{12}\text{CH}_4$, $^{13}\text{CH}_4$, CO_2 , and H_2O in a 70 Torr sample of a healthy 28-year-old individual. The concentration of methane of 1.87 ppm was obtained by fitting the measured absorption spectrum with the data from the HITRAN database.⁷⁶ For a subject with suspected intestinal bacterial overgrowth [Fig. 8(b)], a much higher methane concentration of 11.54 ppm was observed. The absorption peak of $^{12}\text{CH}_4$ is significantly larger than that of $^{13}\text{CH}_4$ since the natural abundances of ^{12}C and ^{13}C are 98.9% and 1.1%, respectively. In these measurements, the filters with Drierite and Ascarite were not used. With the Allan deviation analysis of the presented here CRDS setup, the detection limit was determined to be $2.5 \times 10^{-11} \text{ cm}^{-1}$ with averaging over 70 ringdown events⁹¹ with an estimated fractional detection limit for $^{12}\text{CH}_4$ with the absorption line near 1653.73 nm of about 0.3 ppb. The measured lower values of the CO_2 concentration in Figs. 8(a) and 8(b) are due to the used method of the exhaled breath collection by blowing up a balloon. The air that gets into the airways leading to the lungs (in capnography this volume is called “dead space”) at the end of the inhaling process is expelled first when the exhaling starts.⁹² Since this air does not flow through lungs, it is

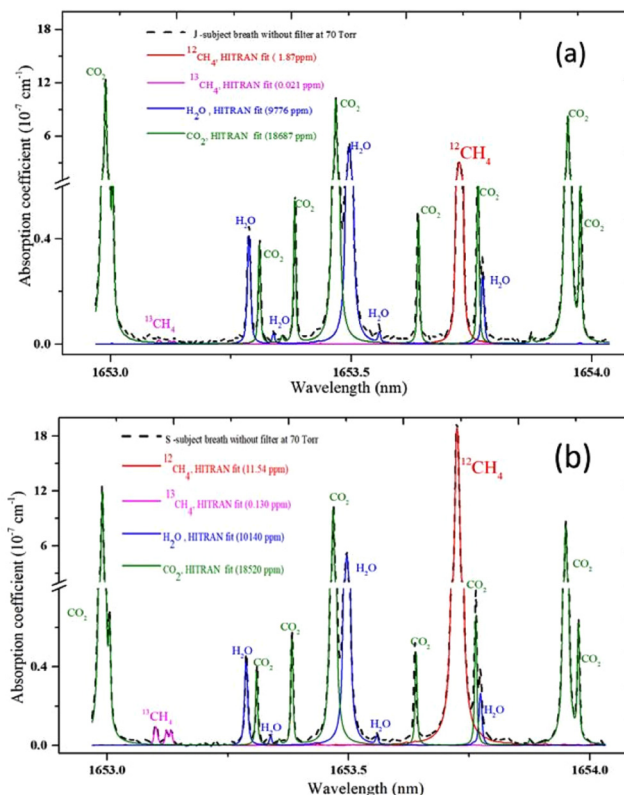


FIG. 8. Absorption spectra: (a) of a healthy 28 years old individual (J-subject) and (b) of a 53-year-old individual with a suspected intestinal bacterial overgrowth (S-subject), showing much higher methane concentration. Data are fitted with the HITRAN database. Larger $^{12}\text{CH}_4$ peaks and much smaller peaks of $^{13}\text{CH}_4$ can be seen.

not enriched with CO_2 , and as a result, the exhaled air in the balloon is diluted with the air from the dead volume having the CO_2 concentration close to the atmospheric one (which is about 400 ppm). The concentration of methane in ambient air is about 1.9 ppm; therefore, when methane is not added to the exhaled breath the concentration close to this atmospheric value is measured. However, for several individuals much higher methane concentrations were registered.

The concentrations of $^{12}\text{CH}_4$ present in the exhaled breath samples of 22 volunteers measured at a pressure in the cavity of 70 Torr are presented in Fig. 9. A concentration above 10 ppm of methane is considered positive in the diagnosis of small intestinal bacterial overgrowth.⁹³ The results of Fig. 9 indicate that 3 out of 22 participants had this criterion fulfilled. Two subjects had somewhat elevated level of methane but below 10 ppm. For all other subjects, the $^{12}\text{CH}_4$ concentration was within 1.8–2 ppm.

E. Progress of CRDS in the mid-IR and novel trends

Mid-IR systems being able to exploit high absorption cross sections encounter restraints, such as lower performance and

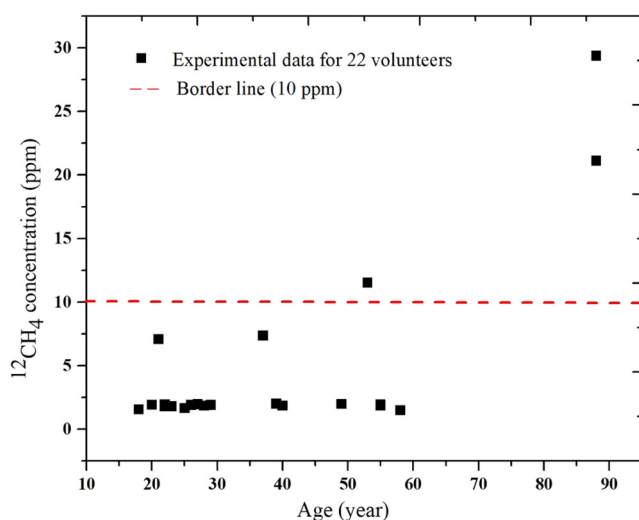


FIG. 9. ¹²CH₄ concentrations for 22 volunteers of different ages. Concentration values above the red dashed line can indicate abnormal gastrointestinal condition.

higher costs of required components compared to the near-IR. Cavity ringdown spectra of ammonia at 10 ppbv were recorded with a CW DFB QCL at 8.5 μm with a detection limit for ammonia reaching 0.25 ppbv.⁹⁴ A CRDS instrument based on a widely tunable between 6 and 8 μm optical parametric oscillator was developed for the detection of vapor-phase explosives with the detection limit down to 75 ppt.⁹⁵ Another CRDS system with a DFB QCL near 4.5 μm actively stabilized to a given cavity mode achieved the minimum detectable absorption of $2.3 \times 10^{-11} \text{ cm}^{-1}$.⁹⁶ A linewidth reduction as well as the locking of a DFB QCL wavelength near 4.527 μm with an optical frequency comb via optical feedback with a CRDS setup targeting radiocarbon detection using ¹⁴C¹⁶O₂ absorption line proved a 100 kHz resolution bandwidth and the ability to detect radiocarbon at ¹⁴C/¹²C isotope ratio of $\sim 10^{-8}$.⁹⁷

A frequency-stabilized CRDS technique with combined high-bandwidth locking of a continuous-wave probe laser and a frequency-stabilized cavity leads to a significant improvement of the SNR⁹⁸ and a better limit of detection ($1.7 \times 10^{-11} \text{ cm}^{-1}$ after averaging 170 ringdown events requiring 21 ms at an acquisition rate of 8 kHz).⁹⁹ The introduction of an optical feedback frequency-stabilized CRDS¹⁰⁰ allowed us to reduce the baseline noise to $5 \times 10^{-12} \text{ cm}^{-1}$. Maity *et al.* utilized a quantum cascade laser tunable in the mid-IR range 7.5–8 μm with a power $\sim 100 \text{ mW}$ coupled with a CRDS setup to obtain the detection limit of methane isotopes in air $\sim 13 \text{ ppb}$ and $\sim 0.0003 \text{ cm}^{-1}$ resolution.¹⁰¹ The advantage of locking the probe laser frequency to a self-referenced femtosecond optical frequency comb and a high acquisition rate was recently demonstrated,¹⁰² resulting in the reduced noise-equivalent absorption coefficient of $2 \times 10^{-12} \text{ cm}^{-1} \text{ Hz}^{-1/2}$. A way to overcome the CRDS limitation of measuring only one resonant cavity mode at a given time by realizing a broadband dual frequency comb CRDS was proposed by

Lisak *et al.*¹⁰³ Further development of this trend of combining the advantages of the CRDS and frequency comb techniques can be expected also in the future.

IV. FREQUENCY COMB SPECTROSCOPY (FCS)

Back in the 1970s, Eckstein *et al.* identified the comb structure of the Fourier transformed spectrum from a picosecond laser pulse train and used it to study the atomic spectra.¹⁰⁴ Near the end of the 1990s, with the invention of the self-referencing technique, the femtosecond frequency comb was first demonstrated in the Kerr lens mode-locked Ti:sapphire laser and revolutionized the field of optical metrology following pioneering works by two research groups of Hänsch and Hall.^{105–107} The frequency comb coherently unites the electromagnetic spectrum from the radio frequency to the optical frequency with a simple expression $f_n = nf_r + f_0$, where optical frequencies f_n are the equally spaced comb teeth, which are under the broad spectrum of a single pulse; f_r is the frequency gap between the adjacent comb teeth and is equivalent to the pulse repetition rate or the reciprocal of the pulse interval; and f_0 is the carrier-envelope offset frequency, related to the pulse-to-pulse carrier-envelope phase slippage of the phase-coherent pulse train.¹⁰⁸ For ordinary mode-locked lasers, f_r is usually in the range between 50 MHz to 1 GHz, which is determined by the optical length of the round trip in the laser resonator. With pulse picking or cavity filtering techniques, f_r can be extended to the range of the order from 0.001 to 10 GHz. f_0 is in the range between 0 to f_r due to the offset between the comb teeth and the integer number multiplied by the repetition rate. Hence, if the coherent laser pulse train is in the near infrared, the integer n is of the order of 10^4 – 10^7 to bridge the gap from the radio frequency to the near infrared optical frequency. With a commercially available radio frequency reference, such as the Rb standard, and the precise control of the f_r and f_0 by phase locked loops, the clockwork mechanism of the frequency comb transfers the stability of the frequency standard from the radio frequency to the optical frequency. Hence, for a Ti:sapphire femtosecond laser emitting the pulse train of a 100 MHz repetition rate with 10 fs pulse duration, the corresponding frequency comb covers about 100 THz spectral range containing 10^6 comb teeth, and each comb tooth can be regarded as a narrow-linewidth continuous-wave laser.

The mode-locked laser sources have played a major role in the developments and applications of the frequency comb. Various types of the mode-locked solid-state lasers and fiber lasers have been stabilized to radio frequency standards to serve numerous applications.¹⁰⁹ With the implementation of nonlinear wavelength conversion techniques such as supercontinuum, second or high harmonic, sum or difference frequency generation, four-wave mixing, etc., frequency combs based on mode-locked lasers cover the electromagnetic spectrum from the extreme ultraviolet to the terahertz range, enabling the bidirectional phase-coherent conversion between these frequencies and radio frequencies and continuously finding new applications, such as ultrastable clock, ultrasensitive sensing, and ultraprecise spectroscopy.¹⁰⁹

In addition to the mode-locked lasers as the workhorses for the optical frequency comb community, the electro-optic combs and microresonator frequency combs are being developed

fast.^{110,111} Usually, both latter techniques employ a continuous-wave seed laser with a narrow linewidth. For an electro-optic comb, a seed laser beam is modulated by an electro-optic modulator in phase or both in phase and amplitude to generate a series of sidebands with equal frequency spacing.¹¹⁰ The bandwidth of the modern commercial electro-optic modulators can reach 40 GHz and above. Thus, this method provides wider spacing comb teeth than the mode-locked laser, but the comb bandwidth is usually limited by the electro-optical properties of the modulator. For a microresonator frequency comb, a seed laser beam is coupled into an optical microcavity of high-quality factor to generate the frequency comb by the nonlinear Kerr effect, i.e., four-wave mixing. Due to the interplay between the nonlinearity and dispersion, a stable soliton can circulate in the microresonator with a round trip time in the range of 1–100 ps.¹¹¹ Thus, in the frequency domain, this method can provide a 10 GHz to 1 THz comb spacing and a small volume for the on-chip integration and has already been demonstrated in the sensing and LIDAR applications.^{112,113}

Since the invention at the end of the 20th century, stabilized frequency combs have been widely used for optical clocks,¹¹⁴ frequency metrology,¹¹⁵ laser spectroscopy,¹¹⁶ astronomical spectrum calibration,¹¹⁷ optical communication,¹¹⁸ absolute ranging,¹¹⁹ and other fields. In the field of spectroscopy, frequency combs not only provide super-accurate references for tunable narrow-linewidth lasers by measuring beating signals but also serve as broadband light sources with accurate comb mode frequencies, which simultaneously enable the broadband and high-frequency resolution spectral measurements. There are a large number of optical frequency combs as light sources advancing research on new types of spectroscopic methods such as direct optical frequency comb spectroscopy, broadband cavity-enhanced frequency comb spectroscopy, Fourier transform spectroscopy with a frequency comb, dual comb spectroscopy, frequency comb Vernier spectroscopy, etc.

A. Direct absorption spectroscopy

As a coherent broadband source, a frequency comb can be used to replace an incoherent broadband source in a traditional absorption spectroscopy setup, which usually consists of a light source, an absorbing sample, and a spectrometer,¹¹⁶ as is illustrated in Fig. 10. In this direction, considerable progress has been achieved and still is underway in the development of the spectrometer capable of high-resolution, high-sensitivity, and broadband spectral measurements with a short acquisition time.

Limited by the spectral resolutions of the traditional spectrometers, such as the Czerny–Turner type monochromator¹²⁰ and the Fourier transform spectrometer,¹²¹ the comb structures of the light sources were difficult to resolve below the 0.5 GHz repetition rate. However, in many gas sensing applications at ambient conditions, the linewidths of the target transitions are larger than 1 GHz. Thus, the requirement of high resolution is relaxed, and sometimes free running frequency combs can be used to achieve reasonable results at a low cost. Moreover, the practical applications can benefit from the coherence of these sources with such properties as low divergence, high brightness, long coherence time, etc. Following the Beer–Lambert law, to increase the sensitivity of the trace gas detection, the usual approach of increasing the interaction length between the light and the absorption sample can be used. In the field applications, with the low divergence of the coherent frequency comb laser beams, the ranging distances of up to several kilometers were demonstrated.^{122–125} This distance scale is complementary to the satellite remote sensing of many hundred kilometers range and the laboratory scale investigations in the range of a few meters, enabling a more detailed middle range gas sensing, which is critical for many applications, such as pollution studies, atmospheric science, etc. In the laboratory, usually a multi-pass cell or a high-finesse resonator can be used to increase the interaction length. The Herriott cell or specially designed multipass cells provide a convenient way to increase the interaction length, but the achieved effective interaction lengths are usually limited by the number of reflections allowed by the design and typically are less than 1 km.¹²⁰

We built a confocal multipass cell with about 580 m path length¹²⁰ and used it with a mid-IR comb source¹²⁶ to analyze the human breath. The experimental setup and the spectroscopic results are presented in Fig. 11. It can be seen that the breath from a patient with colon cancer in Fig. 11(c) contained much more methane than that of a healthy person in Fig. 11(d). The mole fractions retrieved from the fittings of Figs. 11(c) and 11(d) are 12.90 ± 0.04 and 1.97 ± 0.04 ppm for CH_4 and 6500 ± 200 and $16\,700 \pm 200$ ppm for H_2O , respectively. The significant reduction of the H_2O mole fraction in the breath of the colon cancer patient is due to the use of a dry ice-cold trap to reduce the water vapor. Further, the detection limit of methane in human breath is estimated to be about 40 ppb in the experiments within standard deviation. The double pass Czerny–Turner monochromator in the Yokogawa analyzer has a resolution of about 0.10 nm and was set at a measurement speed of about 1.00 nm/s.

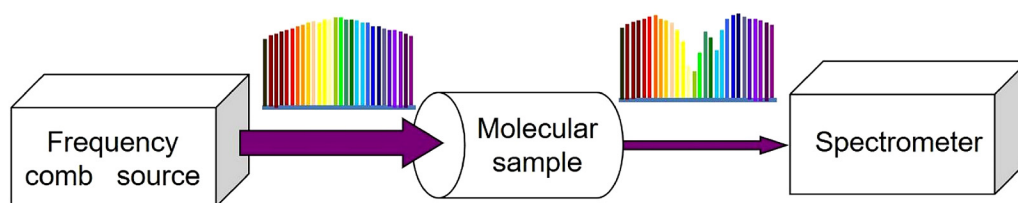


FIG. 10. Scheme of the direct frequency comb absorption spectroscopy.

Even higher sensitivity can be achieved with the cavity-enhanced FCS,^{127–131} employing resonance enhancement with a high-finesse Fabry–Pérot cavity. By actively controlling the length of the Fabry–Pérot cavity, the longitudinal modes of the cavity must be precisely matched with the frequency comb modes, i.e., the pulse interval matches the round trip time for the cavity. Hence, after the round trip in the cavity, the pulse overlaps with the subsequent pulse in time. To ensure all the comb teeth are in constructive interference, the cavity dispersion must be well controlled by the mirror coating, assuring also a high reflectivity, which provides high finesse. With a couple of lenses for the transverse mode matching, the incident frequency comb can have a strong resonance with the high-finesse Fabry–Pérot cavity, which greatly enhances the effective

interaction length. When the resonance is established, the incident pulse can be turned off and the ringdown trace of the comb mode can be analyzed by a dispersion spectrometer with an array of photodiodes.¹²⁷ Alternatively, the Fabry–Pérot cavity can be locked on resonance to the stable frequency comb, and the transmitted light can be analyzed by a Fourier transform, grating based Czerny–Turner or VIPA spectrometer.^{128–131}

The demonstrated broad spectrum ranges of the available frequency combs from the UV to the mid-IR have already covered the majority of spectroscopic gas sensing target molecules. As a result, direct absorption FCS has already found numerous applications, in particular, relevant to environmental monitoring and breath analysis.^{120,129,131}

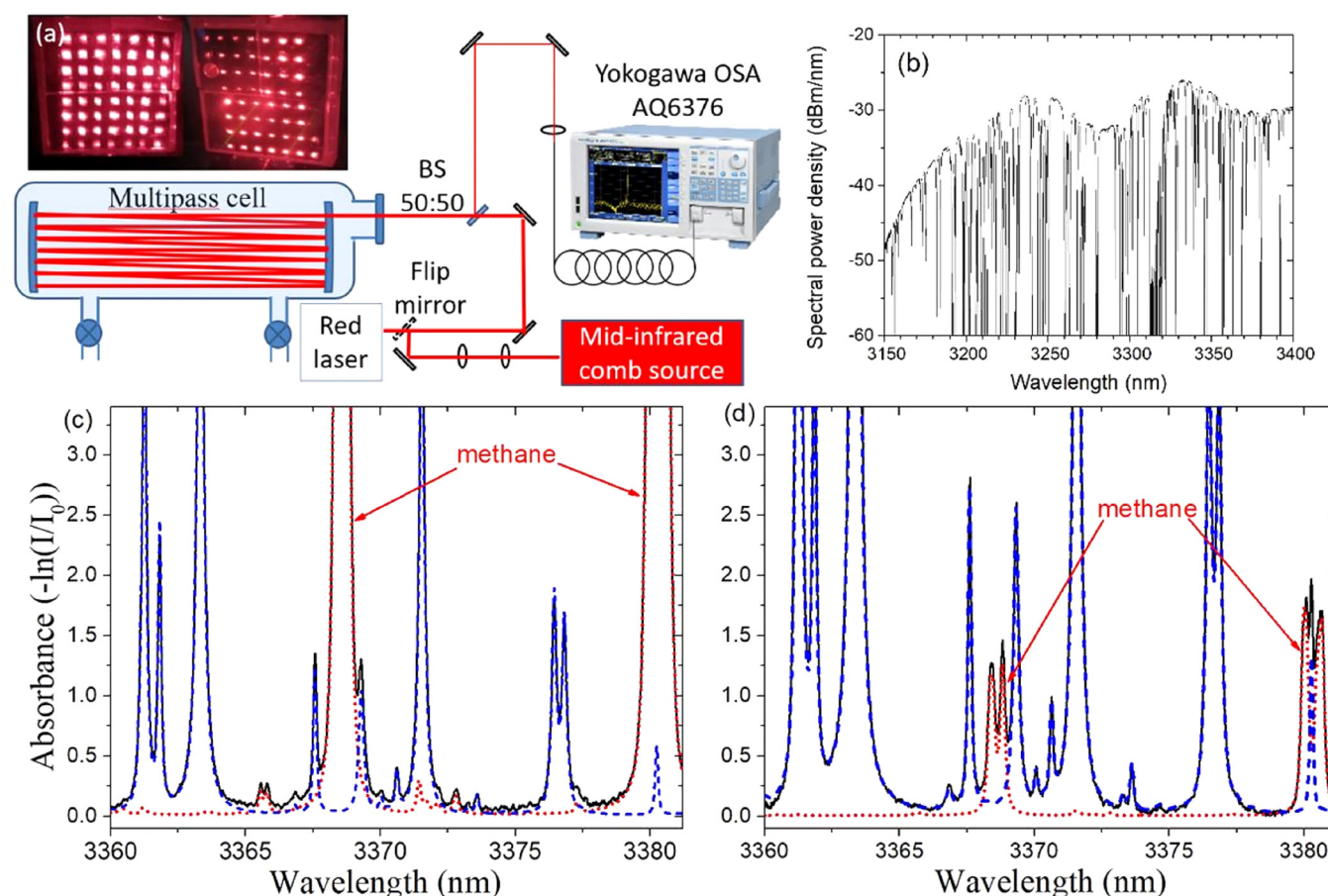


FIG. 11. Direct mid-IR FCS with a multipass cell for breath analysis: (a) Schematic of the experimental setup. A flip mirror is used to let red (He–Ne) laser pass to align the multipass mirror getting the spot patterns, which are shown in the upper left corner. (b) The raw spectrum of the breath from a colon cancer patient was measured by Yokogawa optical spectrum analyzer. Because the signals of many absorption peaks reach the noise floor of -50 dBm/nm determined by the spectrometer and result in large errors in the absorbance calculation, we disregard the absorption peaks above the absorbance value of ~ 3.4 for the HITRAN⁷⁶ simulations and in the concentration retrieving process. (c) and (d) show the normalized absorption spectra (black solid lines) of the exhaled breath from a colon cancer patient and a healthy person, respectively. The methane (red dotted lines) and water vapor (blue dashed lines) are HITRAN simulations presented with the absorption spectra. The CH_4 mole fractions retrieved from the fittings of (c) and (d) are 12.90 ± 0.04 and 1.97 ± 0.04 ppm, respectively. The significant increase of the methane absorption peaks can be seen in (c) at the wavelengths of ~ 3368 and ~ 3380 nm.

B. Dual frequency comb spectroscopy (DFCS)

In 2002, Schiller proposed a novel type of spectrometer utilizing the properties of heterodyning of two frequency combs with a small difference (δ) in the repetition rate.¹³² In 2004, Keilmann *et al.* demonstrated DFCS in the mid-infrared range.¹³³ In 2008, Coddington *et al.* achieved the comb teeth resolution of the DFCS by absolutely locking the dual combs to two stabilized continuous-wave lasers and maintaining the mutual coherence between dual combs.¹³⁴ Several adaptive sampling schemes were proposed to eliminate the requirements of the ultra-stable continuous-wave lasers.^{135–137} Moreover, multi-dimensional dual comb methods were demonstrated to study the coupling of the transition resonance.^{138,139} By using the direction, polarization, or wavelength multiplexing, one femtosecond laser could be used to convert to a dual comb source.^{140–142} Further, with the development of the electro-optic comb and micro-resonator comb, the DFCS was demonstrated with these two types of comb sources in the gas sensing and ranging applications.^{143–146}

There is a notable analogy between DFCS and Fourier transform spectroscopy. For Fourier transform spectroscopy, the light beam (either incoherent or coherent) is divided into two beams after passing through the 50:50 beam splitter: one beam is reflected by a fixed mirror and has a constant path length and the other beam is reflected by a moving mirror and goes over a changing path length. The two light beams finally overlap in space at a photodetector. The photodetector records the interferogram, which is the two beams superposition intensity vs the changing path length and can be Fourier transferred to the spectral domain. The spectral resolution of the traditional Fourier transform spectroscopy is usually determined by the total of the changing path length, and the spectral range depends on the actual sampling rate of the interferogram. Thus, the velocity and total displacement of the moving

mirror are critical for the quality of the spectroscopic measurement. For the usual implementation of the DFCS, two frequency combs with slightly different repetition rates are utilized and no moving parts are involved. The basic working principle is illustrated in Fig. 12.

In the time domain, the pulses emitted by two frequency comb sources form pulse pairs. Because of the slightly different repetition rates of the pulse trains, each pulse pair impinges on the fast photodetector with a linearly incremental time delay. When the pulses in a pair are exactly coincident on the photodetector, just like the zero-path difference in the traditional Fourier transform spectroscopy, the constructive interference gives the center burst of an interferogram. Subsequent pulse pairs arrive on the photodetector with a linearly increasing time delay, analogous to the delay introduced by the moving mirror with constant velocity in Fourier transform spectroscopy. Because pulse pairs constantly move through each other, a new interferogram begins to form after the previous one is finished with a rate equal to the repetition rate difference δ . In the frequency domain, the pulse trains of the two sources form two sets of comb lines with slightly different comb spacing. Comb lines beat with each other. A lowpass filter from DC to $f_r/2$ rejects the beat frequencies of the higher orders other than the adjacent comb modes. Hence, the absorption information carried in optical frequency is downconverted to the radio frequency range, which is just the Fourier transform of the interferogram series. To obtain the spectrum in the optical domain, the radio frequency needs to be upconverted by the f_r/δ factor.

We set up the mid-IR DFCS with a multipass cell to detect acetone, one of the volatile organic compounds considered as a biomarker of diabetes.^{82,83} The experimental setup and the measured spectrum are presented in Fig. 13. The difference frequency generated mid-IR combs are carrier-envelope offset-free.¹²⁶ We designed

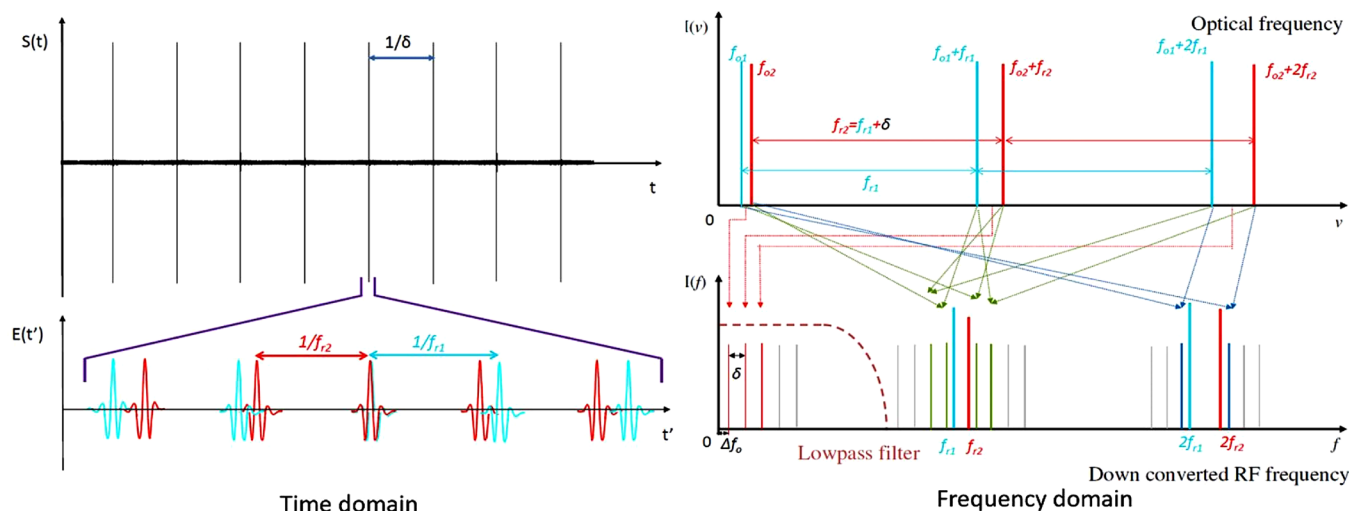


FIG. 12. Principle of the dual frequency comb spectroscopy. For two frequency combs, $f_{1n} = nf_{r1} + f_{o1}$ (blue) and $f_{2n} = nf_{r2} + f_{o2}$ (red), the slight difference of the repetition rates of the dual comb is $\delta = f_{r2} - f_{r1}$. In the time domain, the $S(t)$ is the repeated interferogram with an update rate δ . In the frequency domain, beat notes in the RF range between the optical comb teeth with the nearby order can be filtered by a lowpass filter, which is usually from DC to $f_r/2$.

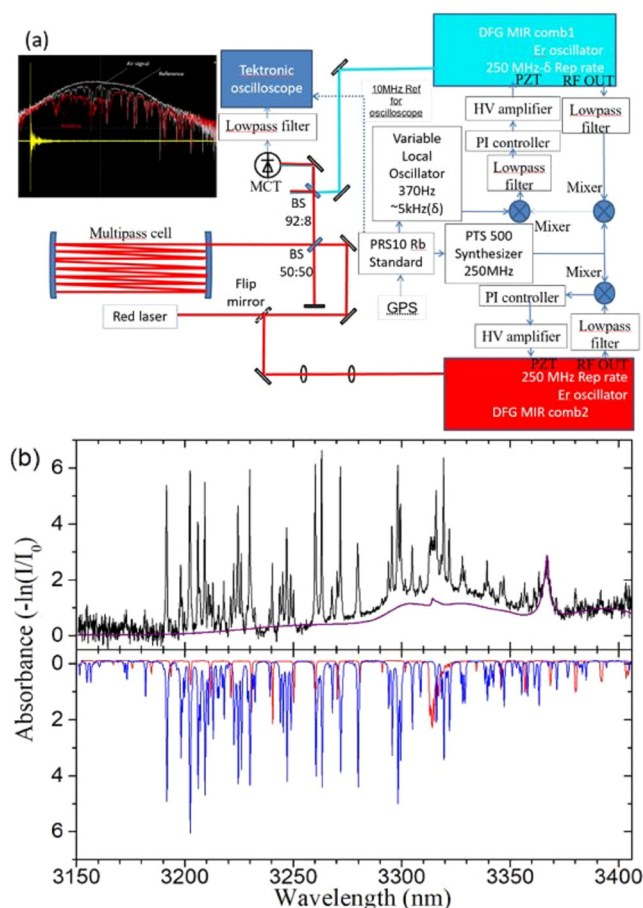


FIG. 13. The experimental setup and the spectroscopic results of mid-IR DFCS for acetone detection. In (a), a screen image of the oscilloscope is presented. The yellow trace is the interferogram averaged over 80 ms. The gray traces are the FFT spectra of the reference and air. The red trace is the FFT spectrum of the acetone mixture. The top panel of (b) shows the normalized absorption spectrum (black) of mixture of 15.0 ± 0.8 ppm acetone in air and PNPL simulation (purple) of 15 ppm acetone. The methane (red) and water vapor (blue) HITRAN⁶ simulations are inverted in the bottom panel of (b) for viewing clarity. The CH_4 and H_2O mole fractions retrieved from the fittings are 1.9 ± 0.1 and 3500 ± 200 ppm, respectively. The detection limit of acetone is estimated to be about 0.8 ppm in 80 ms measurement time with a resolution of 0.3 nm.

the electronics to lock the repetition rates of dual combs with a small difference δ . With the fast Fourier transform performed by a digital oscilloscope, the spectrum can be viewed almost in real time.

It is worth noting that since the measurement principle of the dual frequency comb is that the pulse pairs emitted from the two frequency comb sources are interfering with each other and are asynchronously sampled, this means that essentially the cross correlation measurement of the pulse pairs is performed.

Thus, if the coherence between the two optical combs is degraded over time, it would cause serious distortion of the

interferogram and the FFT spectrum. Indeed, in this case, the average of distorted interferograms would lead to a degraded signal-to-noise ratio and reduced sensitivity of the measurement. Although the frequency comb-locked to radio frequency reference has demonstrated excellent performance in many applications, its short-term stability is limited by that of the RF reference itself, which usually is about 10^{-11} – 10^{-12} in 1 s. Under these circumstances, the comb teeth of a visible comb source would have a line-width of $\sim 5 \times 10^3$ – 5×10^2 Hz in 1 s, which is comparable to the usual repetition rate difference δ . Hence, any noise in combs (f_r or f_o noise) would cause the interferogram distortion within a few tens of milliseconds, and, consequently, the DFCS referenced to a commercial RF reference cannot reach the single comb line resolution.

To overcome this difficulty of maintaining the coherence of the two frequency combs, several schemes are demonstrated. One scheme is that the high degree mutual coherence in seconds can be maintained by locking the frequency comb to ultra-stable continuous-wave lasers. Thus, the distortion of the interferogram is eliminated, and the coherent averaging over seconds can be implemented.^{144,147} The second scheme is to track and record the timing jitter and phase fluctuations of the frequency combs and use them through mixing and redefining the interferogram acquisition time grid to eliminate interferogram distortion and achieve effective coherent averaging.^{135–137,148} The third way is to generate two frequency combs from the same laser resonator, in which case they have an intrinsic coherence. By using multiplexing technology in direction, polarization, wavelength, and transmission path, two mutually coherent pulse trains with a small repetition rate difference can be produced in one resonator, and demonstration experiments have been carried out.^{140–142,149–151}

As a new type of spectral detection method under active development, DFCS is used to identify the species, their structure, and concentration by detecting the spectral response and analyzing it with already known spectral information. Based on the mode-locked lasers, such as solid-state lasers and fiber lasers, the comb spectrum can cover the spectral range from UV to mid-IR. The overtone and the fundamental vibrational bands of many important atmospheric constituents, such as CO_2 , CH_4 , C_2H_6 , CH_3COCH_3 , etc., have been investigated with the DFCS. The cavity-enhanced technique has been used to improve the detection sensitivity.^{152,153} Sensitive and reliable field detections of greenhouse gases have been demonstrated.^{122–125} However, for remote detection, the range of the existing dual comb spectrometers is relatively short, and also only the averaged values through the whole optical path can be measured. Therefore, high power frequency comb sources need to be developed in the future to increase the detection range, especially in the mid- to far-IR regions to increase the sensitivity and expand the detection to a multitude of the molecular species. Improvements in the detection techniques in combination with the comb ranging and LIDAR approaches possibly will lead to the development of distance-resolved atmospheric trace gas analyses that will have a great impact on the development of trace gas monitoring.^{154,155}

Successful implementation of dual frequency comb spectroscopy for atmospheric sensing has promoted its rapid application to many other fields, such as materials science, biochemistry, combustion, food safety, and drug research and development.^{156–160}

The samples to be investigated also vary considerably from gas phase to liquid or solid phase with more complicated transmission spectra and various refractive indexes.^{158,160} In addition, on the basis of non-linear interaction between light and matter, dual frequency comb spectroscopies were also developed to measure the two-photon absorption spectra and analyze multi-component species of biochemical materials and organic substances with a coherent Raman scheme.^{157,159,161,162} Moreover, with the development of the electro-optic and micro-resonator combs, more novel applications with on-chip integration potential are emerging.^{110–113,118,144–146} In short, the DFCS technology is rapidly developing, and it can be foreseen that with the increase of the pulse intensity in the combs and employment of nonlinear optical interactions, the applications of dual frequency comb spectroscopy will be further extended.

C. Vernier spectroscopy

Vernier spectroscopy exploits the optical mode structure of a high-finesse cavity to provide both extended optical path length as well as high spectral resolution detection. Just as with CW cavity ringdown spectroscopy, a resonant optical cavity provides a multiplication of the interaction length between the laser light and the gas sample, and in addition, the mode structure of the cavity is used for spectral filtering. This filtering action is advantageous as it yields a higher effective comb repetition rate, which can easily be resolved with a simple diffraction grating, while still retaining the ability to resolve spectral features at the lower repetition rate.

The coupling of a frequency comb into an optical cavity is more complex than for a CW laser, which, apart from the transverse intensity profile matching, only requires that the laser light matches one of the resonant frequencies of the cavity. Coupling of frequency comb modes into a cavity requires that the cavity-free spectral range matches the repetition rate of the comb, a task which is further complicated by the fact that the cavity modes are not evenly spaced in the presence of dispersion, a result of both the cavity mirror coatings and the presence of an absorber in the cavity. This dispersion imposes additional constraints on the carrier-envelope offset frequency of the comb. Vernier filtering¹⁶³ is the result of intentionally mismatching the comb repetition rate to the free spectral range of the cavity to form a moiré pattern of transmissions that are much more widely spaced than either the comb modes or the cavity free spectral range.

A high-finesse optical resonator has resonances that are spaced by the free spectral range $\text{FSR} = 2\pi c/(n_r L)$, where n_r is the effective refractive index, and L is the round trip length of the optical cavity. Vernier filtering takes place when every m th frequency comb mode is resonant with every n th cavity resonance by appropriate choice of the cavity length.¹⁶³ It is standard to choose the cavity length in analogy with the scales on a Vernier caliper such that $n = m - 1$ ($n \gg 1$ and integer). This choice yields a resonator length that is nearly the same as a perfectly matched resonator, where the free spectral range of the cavity is equal to the repetition rate of the comb, which is advantageous to account for the induced mismatch, because a cavity mirror can then be displaced a known distance from this length using a small translation stage.

We define the Vernier ratio as the ratio between the cavity-free spectral range and the comb repetition rate $\text{FSR}/f_{\text{rep}}$. We can choose this ratio to be of the form

$$\frac{\text{FSR}}{f_{\text{rep}}} = \frac{m}{m-1}. \quad (13)$$

The transmission for an optical cavity can be written as

$$H(\nu) = \frac{H_{\text{max}}}{1 + \left(\frac{2F}{\pi}\right)^2 \sin^2\left[\frac{\phi(\nu)}{2}\right]}. \quad (14)$$

Here, $F = \pi\sqrt{R}/(1-R)$ is the finesse of the cavity, defined by the mirror reflectivity R . $H_{\text{max}} = T^2/(1-R)^2$ is the maximum transmission, accounting for the product of all input and output couplers; T is the mirror transmission. The phase accumulated for a round trip in the cavity in the absence of absorption or dispersion is $\phi(\nu) = 2\pi\nu L n_r/c - \phi_0$, where ϕ_0 is a constant phase shift of the cavity. The function $H(\nu)$ has maxima where $\phi(\nu) = n \cdot 2\pi$. In order to perfectly couple a comb to the resonance of the cavity, we have the condition

$$2\pi(n f_{\text{rep}} + f_{\text{ceo}})L_{\text{rep}} n_r/c - \phi_0 = n \cdot 2\pi. \quad (15)$$

For a comb of a particular repetition rate, we need to set the cavity length to be $L_{\text{rep}} = c/(n_r f_{\text{rep}})$, and the laser carrier-envelope offset frequency to be $f_{\text{ceo}} = (\phi_0/2\pi) \cdot f_{\text{rep}}$. This corresponds to the case where the frequencies of the comb teeth are landing on the maxima of the cavity transmission function of Eq. (14).

When the matching condition of Eq. (13) is fulfilled, every m th comb mode coincides with a maximum of the cavity transmission given by Eq. (14). This yields an output from the cavity, which is similar to that of a comb having a repetition rate of m times the original repetition rate, as can be seen in Fig. 14. For a large cavity finesse, we can assume that only one comb mode is transmitted on each cavity resonance, and the condition of Eq. (13) holds. The transmission function for a comb coupled to a cavity having a lower finesse has been explored elsewhere.¹⁶⁴

1. Highly parallelized data acquisition

The Vernier matching condition of Eq. (13) gives a cavity transmission, such that every m th comb mode is transmitted. As the cavity round trip length is continuously increased or decreased (by about one wavelength) compared to the length satisfying exactly this condition, then the next set of every m th modes will be transmitted. This cavity length scanning allows all modes to be transmitted in groups that can be easily resolved by a diffraction grating.

Detection of the transmitted comb modes is performed using a spectrometer of sufficient resolving power to detect the cavity filtered comb modes. For larger Vernier orders, this is easily done using a dispersive type spectrometer which gives spatial separation of the different wavelengths output from the optical cavity. This approach lends itself to parallel acquisition using 2D detectors such as a camera or focal plane array detector. The light transmitted from the cavity can be dispersed in one spatial direction across a 2D sensor

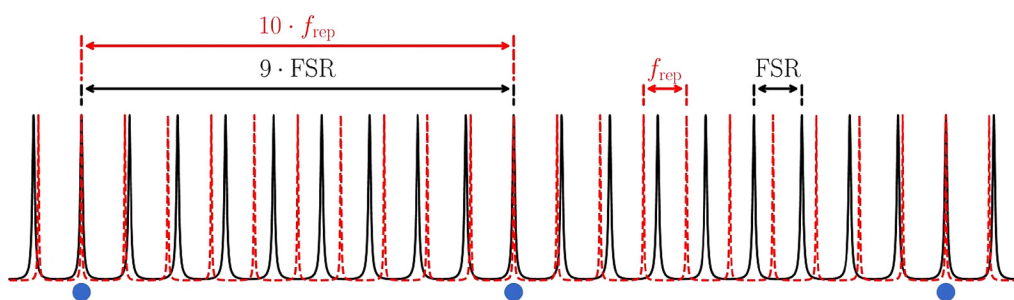


FIG. 14. Vernier filtering scheme for $\text{FSR}/f_{\text{rep}} = 10/9$. Red dashed lines are frequency comb modes and black solid lines are cavity resonant modes. Large blue dots mark the transmitted comb modes, forming regularly spaced intervals, which are larger than both the cavity free spectral range and the comb repetition rate.

and then swept across the perpendicular direction using a movable mirror. This can yield rapid measurement times of less than 1 s.¹⁶⁷

The Vernier filtered output from the cavity can be detected serially using a single photodetector^{164–166} or in parallel using a focal plane array detector.^{163,167} In Ref. 168, a Fourier transform spectrometer was used to measure the output of an enhancement cavity locked to the output of a frequency comb laser. Even higher sensitivity of the Vernier spectroscopy approach can be expected when using a mid-IR frequency comb.¹²⁶

2. Experimental setup

A femtosecond erbium fiber laser (Menlo Systems GmbH, M-Fiber) was used as a frequency comb source with a repetition rate stabilized to 250 MHz and consisted of a separate oscillator and amplifier (see the setup schematic in Fig. 15). The output of the amplifier was broadened using a highly nonlinear fiber to generate a comb spectrum ranging from 1500 nm to 1700 nm. The light from the comb was mode-matched to a scanning high-finesse

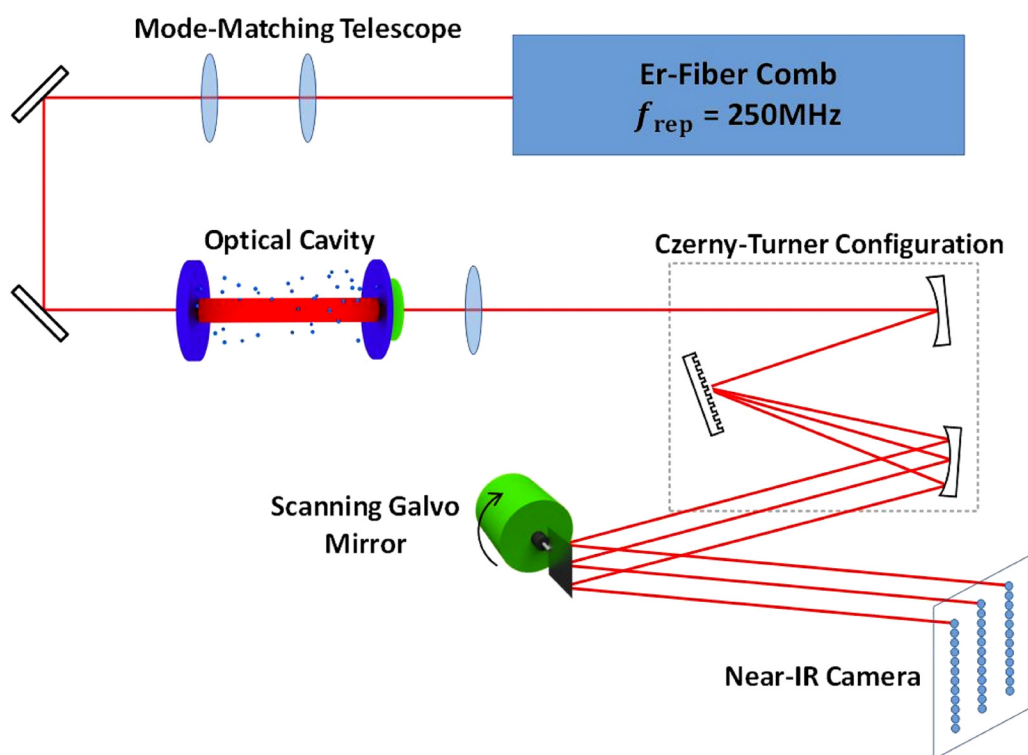


FIG. 15. Setup for Vernier spectroscopy. Light from the comb is mode-matched to the optical cavity, which is displaced from perfect repetition rate matching using a high-resolution translational stage (not shown). A piezoelectric transducer and a galvo mounted tilt mirror (both shown in green) move synchronously to map the different groups of comb modes onto different positions on the detector image.

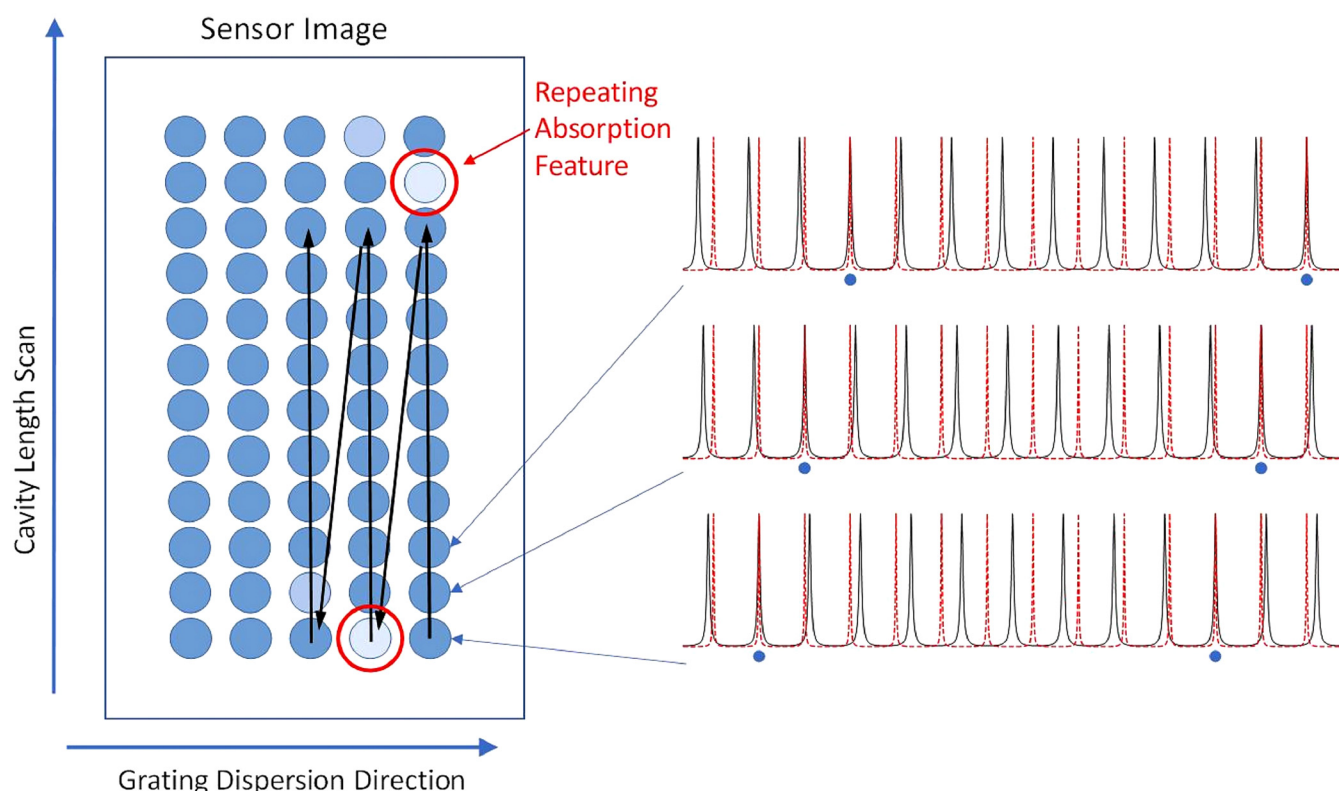


FIG. 16. Formation of 2D image. The grating is oriented to disperse the light in the horizontal direction of the image, yielding the horizontal rows of spots. As the cavity length is changed, the cavity transmission has many overlaps with the comb structure of the laser, which is mapped onto the image by the tilting mirror (shown in vertical direction). This produces the vertical columns of spots on the image, which allows counting of individual comb modes. Scanning the cavity length far enough causes the cavity-comb transmission to repeat, yielding repeating absorption features. These repeating features can be used as a guide to unwrap the image into a spectrum in the manner shown by the black arrows.

Fabry-Pérot cavity consisting of two high reflectivity mirrors (Layertec GmbH), one being flat and the other concave with a 2 m radius of curvature. The high mirror reflectivity yields a cavity finesse of $\sim 30\,000$, which was confirmed with a cavity ringdown measurement. In order to precisely control cavity length and impose different Vernier ratios, the flat mirror was mounted on a high precision motorized translational stage (Newport, GTS150). The concave mirror was mounted on a piezoelectric transducer (PZT) in order to provide fast cavity length changes of larger than one wavelength.

The detector used was a 512×640 InGaAs focal plane array (Princeton Instruments, PIoNIR 640) with a pixel size of $20 \times 20 \mu\text{m}^2$. The detector was cooled thermoelectrically to -80°C to reduce the dark current. Light was dispersed in the horizontal image direction of this detector using a homebuilt Czerny-Turner spectrometer incorporating a $5 \times 5 \text{ cm}^2$, 300 grooves per millimeter gold coated grating (McPherson). Using a tilt mirror mounted to a galvanometer, dispersed light was streaked across the detector in the vertical image direction (Fig. 16). This was done synchronously with the changing cavity length provided by the piezoelectric

transducer such that the different groups of filtered comb modes from the cavity were mapped in the vertical image direction. Additionally, the exposure time of the InGaAs camera was synchronized with the cavity scan and galvo mirror tilt to yield scans recorded in a single image.

3. Results

Shown in Fig. 17 are images that we obtained on the focal plane array detector for a cavity filled with 5 ppm acetylene and the empty cavity. The vertical image direction is the sweep direction of the tilt mirror mounted on a galvo. The horizontal direction is the grating dispersion direction. Acetylene spectrum obtained from the images of Fig. 17 is shown in Fig. 18 together with the calculated HITRAN fit. The observed absorption spectrum shown in Fig. 18 is in good agreement with previously published,¹⁶⁷ however, it is slightly reduced in amplitude compared to the HITRAN simulation of 5 ppmv acetylene. The probable reason is that the absorption that results from the application of Eq. (16) is dependent on any wavelength variation of the cavity mirror reflectivity, as this term

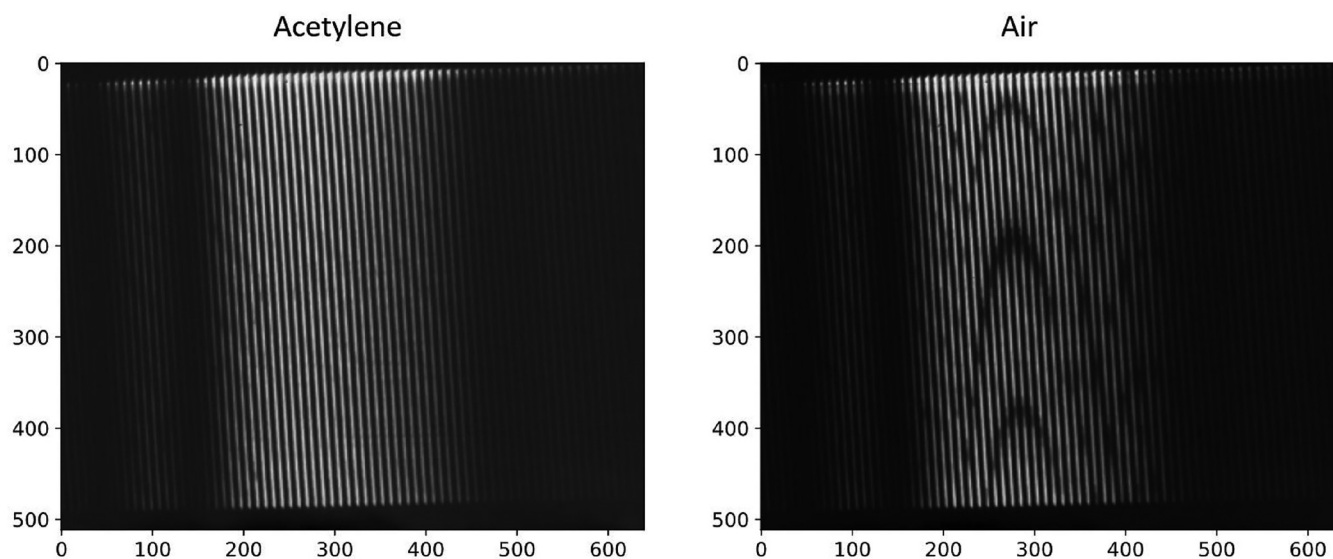


FIG. 17. Images recorded using InGaAs camera for a Vernier ratio of 500/499. The image on the left is the reference image, taken in ambient air. The right image shows absorptions from the $\nu_1 + \nu_3$ band of acetylene at 5 ppm concentration.

determines the effective interaction length with the sample. The wavelength dependent reflectivity of the mirrors in our cavity was not fully characterized for the entire wavelength region shown and as a result, the amplitudes of the peaks in the long wavelength region are somewhat reduced compared to the shorter wavelength peaks. The achieved absorption sensitivity is about $8 \times 10^{-8} \text{ cm}^{-1} \text{ Hz}^{-1/2}$, corresponding to a detection limit of about

70 ppbv for acetylene. The spectral resolution is about 1.1 GHz in single images taken in 0.5 s, and the wavelength range is between 1510 to 1550 nm.

The density of spectral information is high in these images. The spots depicted in Fig. 17 have been smeared into vertical bands, as the individual spots do not occupy enough pixels on the image to be resolvable. However, using repeating absorption

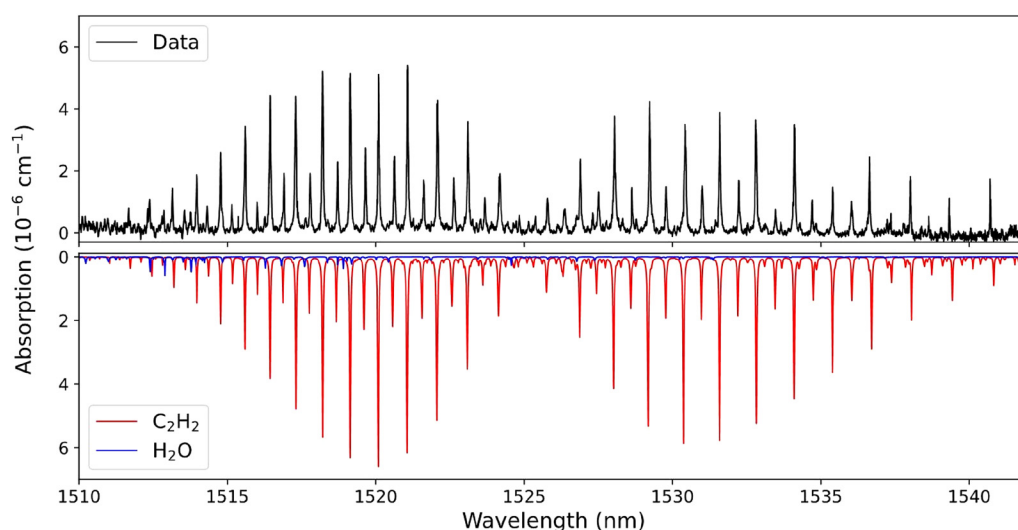


FIG. 18. Acetylene spectrum obtained from the images of Fig. 17 for a Vernier ratio of 500/499 (top). This is compared to line shapes simulated from the HITRAN database for 5 ppm of acetylene at 1 atm pressure and 296 K and shown in red with the inverted axis (bottom).

features, we were able to successfully recover the spectrum of acetylene by dividing each vertical band into a number of banks corresponding to the Vernier number m . The pixels in each of these banks were summed to yield a measure of the integrated intensity, which was performed both when the cavity contained ambient air and acetylene. Equivalent image positions were used to evaluate the fractional change in intensity between the cavity containing an absorber and the cavity containing ambient air. This fractional intensity change can be related to the absorption coefficient by¹⁶⁹

$$\alpha = -\frac{1}{L} \ln \left[\frac{1}{R^2} \left(1 - \frac{1-R^2}{1-\Delta I/I_0} \right) \right]. \quad (16)$$

Here, L is the round trip cavity length, R is the mirror reflectivity, and $\Delta I/I_0$ is the fractional change in intensity.

In order to calibrate the wavelength of the resulting spectrum, it is required that a known absorption feature be present in the image, as the frequency spacing can be found by counting the resolved spots in the image. In our case, since the individual comb modes were not resolved, two absorption features were used to calibrate the wavelength scale. However, when the spots can be resolved with enough image pixels, phase information can be retrieved from fits to the spot shapes.¹⁶³

D. Comparison of the characteristics of frequency comb spectrometers and remarks on multicomponent gas analysis

For every spectrometer, the most important specifications are the resolution, sensitivity, bandwidth, and acquisition time. Compared to other spectroscopic techniques, the biggest advantage of the FCS is that these four specifications can achieve high performance simultaneously owing to the remarkable properties of the comb source. However, for each of these specifications, there is no obvious advantage. Therefore, the primary task of the future development for frequency comb spectroscopy is to find the appropriate application and to improve the specifications that are needed for this particular application.

In principle, the spectral sampling of the frequency comb spectroscopy is limited by the repetition rate, which can usually be regarded as the spectral resolution. Therefore, the most direct method to increase the sampling of the frequency comb spectroscopy is to reduce the repetition rate of the comb source. However, the low repetition rate optical comb has a long cavity and is severely affected by environmental disturbances, presenting a significant challenge. There exist two ways to circumvent this difficulty. One approach is implemented by Hébert *et al.*¹⁷⁰ to use the phase-modulated pulse technique of picking one pulse out of many coherent pulses to reduce the repetition rate. Though it increases the spectral resolution, in the time domain, the sampling rate is also decreasing. Hence, the overall bandwidth is limited by the Nyquist law. The other approach is the spectral interleaving by changing the repetition rate in very small steps and stitching spectra with slightly different comb teeth.^{171,172} In theory, the resolution in the interleaving method can break through the comb repetition rate restriction and is only limited by the linewidth of the comb teeth, i.e., the reciprocal of the coherence time of the pulse

train. But this method requires a significant increase in the acquisition time to collect multiple sets of spectra, which cannot meet the real-time or onsite requirements of many applications.

The detection sensitivity of a spectrometer can usually be concluded from the signal-to-noise ratio of the spectrum of a gas standard. The major factors affecting the signal-to-noise ratio in the FCS can be categorized as noise and experimental conditions. Noise includes the additive and multiplicative noise introduced in the measurement process. Additive noise is mainly shot noise, relative intensity noise of the comb sources, and the measurement noise caused by the limited dynamic range of the detector. Multiplicative noise is the relative time jitter and phase noise between two pulse trains in the DFCS. The experimental conditions refer to the acquisition time of the spectrum, the number of spectral elements, the measurement bandwidth, the interaction distance with the sample, and others. To evaluate the experimental results in the DFCS, Newbury *et al.*¹⁷³ proposed the quality factor, which is the product of the signal-to-noise ratio and the number of resolved spectral elements normalized by the square root of the total acquisition time. The quality factors of most demonstrated dual frequency comb spectrometers were around 10^6 – 10^7 Hz^{1/2}.^{173,174} The exception was the measurement with the quality factor of 2×10^8 Hz^{1/2} that was achieved with the continuous coherent averaging of the interferogram for 24 h.¹³⁶ To compare to the traditional spectrometer, the noise-equivalent absorption (NEA) coefficient per spectral element is defined as the absorption sensitivity normalized by the square root of the ratio between the number of resolved spectral elements and the acquisition time. The fractional detection limit of the target molecule normalized by 1 s acquisition time can be estimated as $\text{NEA}/(\sigma_{\text{max}} \cdot n)$, where σ_{max} is the maximum absorption cross section of the target molecular transitions in the detection range for the single resolved spectral element, and n is the number density of the gas mixture. In Table II, the achieved detection characteristics of the frequency comb spectrometers with cavity-enhanced^{128,131,153} or open path^{122,125} configurations for environmental^{122,125} or breath analysis¹³¹ are summarized.

The spectral detection bandwidth is usually limited by the frequency comb source. The development of frequency comb sources from the deep ultraviolet to THz range was progressing at a fast pace.^{175,176} Together with the electro-optic and micro-resonator frequency combs, reliable coherent sources have been adopted for large bandwidth detections. Moreover, the high-performance detectors for different spectral ranges are showing fast improvements,¹⁷⁷ which allow us to expand the variety of target molecules and improve the sensitivity of their detection.

The acquisition time of the FCS is generally short compared to the methods with tunable continuous-wave laser sources. For the direct FCS, the acquisition time is often limited by the spectrometer. While for the DFCS, the single interferogram trace acquisition time is limited by the update rate, which is the repetition rate difference. The spectral detection bandwidth is at most as wide as the pulse bandwidth and is also limited by $\Delta\nu = f_r^2/(2\delta)$ in dual comb setup. Hence, if the desired spectral range is narrower than that provided by the source, the repetition rate difference (δ) can be increased to reduce the acquisition time.¹⁷⁸

With the broadband coherent frequency comb source, the FCS is a natural fit to the multicomponent analysis. There have already

TABLE II. Performance characteristics of the frequency comb spectrometers.

Species	Fractional detection limit	NEA per spectral element ($\text{cm}^{-1} \text{Hz}^{-1/2}$)	SNR@ acquisition time	Resolution (GHz)	Spectral coverage bandwidth@center
CO_2 CO^{153}	12 ppm, 11 ppm	1.5×10^{-8}	189@320 s	0.203	0.35 nm@1570 nm
CO_2	1 ppm	7.3×10^{-10}	588@300 s	0.10	70 nm@1635 nm
CH_4^{122}	3 ppb				
$\text{C}_2\text{H}_2^{167}$	70 ppb	1.2×10^{-9}	70@1 s	1.1	40 nm@1530 nm
$\text{C}_2\text{H}_2^{128}$	2 ppb	3.4×10^{-11}	1000@6s	0.380	30 nm@1530 nm
CH_3COCH_3 $\text{C}_3\text{H}_8\text{O}$	5.7 ppm m, 2.4 ppm m,	2×10^{-9}	10@60s	2.0	400 nm@3400 nm
$\text{C}_2\text{H}_6^{125}$	0.4 ppb				
H_2CO	126 ppt	5×10^{-11}	$\sim 500@6$ s	0.272	160 nm@3480 nm
C_2H_6	378 ppt				
CH_4	644 ppt				
CH_3OH	722 ppt				
OCS	900 ppt				
HDO	1.4 ppb				
C_2H_4	19 ppb				
CS_2	17 ppb				
NH_3	103 ppb				
H_2O^{131}	813 ppb				

been successful applications of the greenhouse gases monitoring, the breath analysis, and so on in different wavelength intervals.^{112,116,120,129,131,122–125} If the target molecular species have sharp absorption features that are not overlapping, the multi-component analysis is straightforward. However, in many cases, the molecules have broad spectral features, and these features overlap. It remains quite challenging to accurately decompose the complicated spectrum to get the correct concentrations of the multispecies. The usual way to tackle this issue starts with the collection of spectra of various separate species in a database. After acquiring the spectrum from a multicomponent sample, many characteristic data points can be determined from the pre-examination of the sample spectrum and used as the input of the analysis model, which calculates the concentration of each component with multivariate data analysis by appropriate algorithms. The popular models include the classic least square method, inverse least square method, principal component regression, partial least squares method, neural network, etc.¹⁷⁹ The first three are mainly for the low gas concentration of each component, so that the absorbance of each component is in the linear regime. The partial least squares method and neural network can achieve the approximation of nonlinear functions, which is suitable also for the retrieval of the high concentrations of the components.

FCS has been successfully used in high-resolution, high-sensitivity, and multi-component real-time atmospheric and breath analysis. In the direction of transferring the laboratory prototype to the field deployable instruments, the microcavity combs together with the nanophotonics will take the instrumentation to the chip scale. With the rapid development of the FCS spectrometers, spectroscopy of single events, kinetics, and microscopy will find applications in many fields such as atmospheric chemistry and respiratory diagnosis.¹¹⁶

V. CONCLUSIONS

In this paper, we considered several spectroscopic techniques for sensitive detection of trace gases in the atmospheric air and in exhaled breath. Wavelength modulation spectroscopy and its application to the detection of acetone and methane were described. Both types of methane measurements point-like with a multipass cell as well as long open-path were described. In view of the relative simplicity, low cost, and robustness, this technique finds numerous applications, including those in the field conditions. WMS sensors for the detection of methane, carbon monoxide, ammonia, acetylene, carbon dioxide, nitrogen oxide, and formaldehyde were reviewed and compared. Overall, the WMS technique shows high potential for the real time, high resolution, and sensitive detection of trace gases.

Cavity ringdown spectroscopy can provide high sensitivity with the detection limit down to ppb and even ppt levels and can directly provide concentration values for target gases. At the same time, this technique does not possess high noise and vibration immunity and requires a very thorough alignment of the system.

A lot of progress in recent years in the field of spectroscopy is related to the development of optical frequency combs. Frequency comb spectroscopy has been successfully used in high-resolution, high-sensitivity, and multi-component real-time atmospheric and breath analysis. Remarkably, such measurements can be performed fast with a broadband wavelength coverage. We presented the results obtained with direct, dual comb, and Vernier frequency comb techniques. Different realizations of the approach were compared by their fractional detection limits, noise-equivalent absorption, spectral resolution, and coverage. Currently, efforts are being made to improve the key performance indicators of spectrometers based on frequency comb sources to meet different application requirements. These include breaking through the resolution limit

imposed by the repetition rate, achieving high sensitivity, which is restricted by the comb and environmental noise, developing frequency comb sources in different electromagnetic wave bands, using parallel detection and other techniques to analyze multicomponent samples, reducing the data acquisition time, etc. At the same time, the development of portable, sensitive, and onsite detection equipment is the primary task for the field applications of frequency comb spectroscopy in the future.

ACKNOWLEDGMENTS

This work was supported by the Robert A. Welch Foundation (Grant No. A1546), the Open Fund of State Key Laboratory of Applied Optics (No. SKLA02020001A12), the Shandong Provincial Key Research and Development Project (No. 2020CXGC010104), and the National Natural Science Foundation of China (Grant No. 12074439).

AUTHOR DECLARATIONS

Conflict of Interest

The authors have no conflict of interest to disclose.

Author Contributions

Jinbao Xia: Investigation (equal); writing – original draft (equal). **Feng Zhu:** Investigation (equal); writing – original draft (equal). **James Bounds:** Investigation (equal); writing – original draft (equal). **Eshtar Aluaue:** Investigation (equal); writing – original draft (equal). **Alexandre Kolomenskii:** Conceptualization (equal); funding acquisition (equal); validation (equal); writing – review & editing (equal). **Qian Dong:** methodology (equal); writing – original draft (equal). **Jingliang He:** funding acquisition (equal); methodology (equal); resources (equal). **Cain Meadows:** writing – original draft (equal). **Sasa Zhang:** funding acquisition (equal); methodology (equal); resources (equal). **Hans Schuessler:** Conceptualization (equal); funding acquisition (equal); methodology (equal); project administration (equal); writing – review & editing (equal).

DATA AVAILABILITY

The data that support the findings of this study are available within the article.

REFERENCES

- ¹H. Huszár, A. Pogany, Z. Bozók, Á. Mohácsi, L. Horváth, and G. Szabó, “Ammonia monitoring at ppb level using photoacoustic spectroscopy for environmental application,” *Sens. Actuators B Chem.* **134**, 1027–1033 (2008).
- ²M. Gabrys, C. Corsi, F. S. Pavone, and M. Inguscio, “Simultaneous detection of CO and CO₂ using a semiconductor DFB diode laser at 1.578 μm ,” *Appl. Phys. B: Lasers Opt.* **65**(1), 75–79 (1997).
- ³M. Basanta, B. Ibrahim, R. Dockry, D. Douce, M. Morris, D. Singh, A. Woodcock, and S. J. Fowler, “Exhaled volatile organic compounds for phenotyping chronic obstructive pulmonary disease: A cross-sectional study,” *Respir. Res.* **13**(1), 72 (2012).
- ⁴L. Ciaffoni, G. Hancock, J. J. Harrison, J.-P. H. van Helden, C. E. Langley, R. Peverall, G. A. D. Ritchie, and S. Wood, “Demonstration of a mid-infrared cavity enhanced absorption spectrometer for breath acetone detection,” *Anal. Chem.* **85**(2), 846–850 (2013).
- ⁵D. S. Bomse, A. C. Stanton, and J. A. Silver, “Frequency modulation and wavelength modulation spectroscopies: Comparison of experimental methods using a lead-salt diode laser,” *Appl. Opt.* **31**(6), 718–731 (1992).
- ⁶J. Y. Li, G. Luo, Z. H. Du, and Y. W. Ma, “Hollow waveguide enhanced dimethyl sulfide sensor based on a 3.3 μm interband cascade laser,” *Sens. Actuators B* **255**, 3550–3557 (2018).
- ⁷K. L. Vodopyanov, *Laser-based Mid-Infrared Sources and Applications* (Wiley, 2020).
- ⁸A. Schliesser, N. Picqué, and T. W. Hänsch, “Mid-infrared frequency combs,” *Nat. Photonics* **6**(7), 440–449 (2012).
- ⁹S. Palzer, “Photoacoustic-based gas sensing: A review,” *Sensors* **20**(9), 2745 (2020).
- ¹⁰D. C. Dumitras, M. Petrus, A.-M. Bratu, and C. Popa, “Applications of near infrared photoacoustic spectroscopy for analysis of human respiration: A review,” *Molecules* **25**(7), 1728 (2020).
- ¹¹P. Patimisco, G. Scamarcio, F. K. Tittel, and V. Spagnolo, “Quartz-enhanced photoacoustic spectroscopy: A review,” *Sensors* **14**(4), 6165–6206 (2014).
- ¹²H. Lin, H. Zheng, B. A. Z. Montano, H. Wu, M. Giglio, A. Sampaolo, P. Patimisco, W. Zhu, Y. Zhong, and L. Dong, “Ppb-level gas detection using on-beam quartz-enhanced photoacoustic spectroscopy based on a 28 kHz tuning fork,” *Photoacoustics* **25**, 100321 (2022).
- ¹³L. Shao, J. Mei, J. Chen, T. Tan, G. Wang, K. Liu, and X. Gao, “Recent advances and applications of off-axis integrated cavity output spectroscopy,” *Microw. Opt. Technol. Lett.* (published online 2022).
- ¹⁴C. Liu and L. Xu, “Laser absorption spectroscopy for combustion diagnosis in reactive flows: A review,” *Appl. Spectrosc. Rev.* **54**(1), 1–44 (2019).
- ¹⁵J. Li, Z. Yu, Z. Du, Y. Ji, and C. Liu, “Standoff chemical detection using laser absorption spectroscopy: A review,” *Remote Sens.* **12**(17), 2771 (2020).
- ¹⁶D. Herriott, H. Kogelnik, and R. Kompfner, “Off-axis paths in spherical mirror interferometers,” *Appl. Opt.* **3**(4), 523–526 (1964).
- ¹⁷E. Gerecht, K. O. Douglass, and D. F. Plusquellic, “Chirped-pulse terahertz spectroscopy for broadband trace gas sensing,” *Opt. Express* **19**, 8973 (2011).
- ¹⁸T. Wei, H. Wu, L. Dong, R. Cui, and S. Jia, “Palm-sized methane TDLAS sensor based on a mini-multi-pass cell and a quartz tuning fork as a thermal detector,” *Opt. Express* **29**(8), 12357–12364 (2021).
- ¹⁹T. Mohamed, F. Zhu, S. Chen, J. Strohaber, A. A. Kolomenskii, A. A. Bengali, and H. A. Schuessler, “Multipass cell based on confocal mirrors for sensitive broadband laser spectroscopy in the near infrared,” *Appl. Opt.* **52**, 7145–7151 (2013).
- ²⁰G. Gervasoni, M. Carminati, and G. Ferrari, “FPGA-based lock-in amplifier with sub-ppm resolution working up to 6 MHz,” in *2016 IEEE International Conference. Electronics, Circuits and Systems (ICECS)* (IEEE, 2016).
- ²¹C. H. Smith, C. S. Goldenstein, and R. K. Hanson, “A scanned-wavelength-modulation absorption-spectroscopy sensor for temperature and H₂O in low-pressure flames,” *Meas. Sci. Technol.* **25**(11), 115501 (2014).
- ²²V. Weldon, J. Gorman, P. Phelan, J. Hegarty, and T. Tanbun-Ek, “H₂S and CO₂ gas sensing using DFB laser diodes emitting at 1.57 μm ,” *Sens. Actuators B* **29**(1–3), 101 (1995).
- ²³G. Wysocki, Y. Bakhrkin, S. So, F. K. Tittel, C. J. Hill, R. Q. Yang, and M. P. Fraser, “Dual interband cascade laser based trace-gas sensor for environmental monitoring,” *Appl. Opt.* **46**(33), 8202 (2007).
- ²⁴J. S. Li, H. Deng, J. Sun, B. L. Yu, and H. Fischer, “Simultaneous atmospheric CO, N₂O and H₂O detection using a single quantum cascade laser sensor based on dual-spectroscopy techniques,” *Sens. Actuators B* **231**, 723–732 (2016).
- ²⁵J. B. Xia, F. Zhu, S. S. Zhang, A. Kolomenskii, and H. A. Schuessler, “A ppb level sensitive sensor for atmospheric methane detection,” *Infrared Phys. Technol.* **86**, 194 (2017).
- ²⁶Q. Gao, Y. Zhang, J. Yu, S. Wu, Z. Zhang, F. Zhang, X. Lou, and W. Guo, “Tunable multi-mode diode laser absorption spectroscopy for methane detection,” *Sens. Actuators A* **199**, 106–110 (2013).
- ²⁷J. Xia, C. Feng, F. Zhu, S. Ye, S. Zhang, A. Kolomenskii, Q. Wang, J. Dong, Z. Wang, W. Jin, and H. A. Schuessler, “A sensitive methane sensor of a ppt

detection level using a mid-infrared interband cascade laser and a long-path multipass cell,” *Sens. Actuators B* **334**, 129641 (2021).

²⁸J. N. Oliaee, N. A. Sabourin, S. A. Festa-Bianchet, J. A. Gupta, M. R. Johnson, K. A. Thomson, G. J. Smallwood, and P. Lobo, “Development of a sub-ppb resolution methane sensor using a GaSb-based DFB diode laser near 3270 nm for fugitive emission measurement,” *ACS Sens.* **7**, 564–572 (2022).

²⁹K. K. Schwarm, C. L. Strand, and V. A. Miller, “Calibration-free breath acetone sensor with interference correction based on wavelength modulation spectroscopy near 8.2 μm ,” *Appl. Phys. B* **126**(1), 1–10 (2020).

³⁰F. Nadeem, J. Mandon, A. Khodabakhsh, S. Cristescu, and F. Harren, “Sensitive spectroscopy of acetone using a widely tunable external-cavity quantum cascade laser,” *Sensors* **18**(7), 2050 (2018).

³¹J. B. Xia, F. Zhu, A. A. Kolomenskii, J. Bounds, S. Zhang, M. Amani, L. J. Fernyhough, and H. A. Schuessler, “Sensitive acetone detection with a mid-IR interband cascade laser and wavelength modulation spectroscopy,” *OSA Contin.* **2**, 640–654 (2019).

³²A. P. M. Michel, D. Miller, K. Sun, L. Tao, L. Stanton, and M. A. Zondlo, “Long-path quantum cascade laser-based sensor for methane measurements,” *J. Atmos. Ocean. Technol.* **33**(11), 2373–2384 (2016).

³³J. B. Xia, F. Zhu, S. S. Zhang, A. Kolomenskii, J. Dong, K. Okada, J. Strohaber, and H. A. Schuessler, “Probing greenhouse gases in turbulent atmosphere by long-range open-path wavelength modulation spectroscopy,” *Opt. Lasers Eng.* **117**, 21–28 (2019).

³⁴A. Schliesser, M. Brehm, F. Keilmann, and D. van der Weide, “Frequency-comb infrared spectrometer for rapid, remote chemical sensing,” *Opt. Express* **13**, 9029–9038 (2005).

³⁵Y. Zhang, J. Ding, X. Zhang, J. Fang, and Y. Zhao, “Open-path sensor based on QCL for atmospheric N_2O measurement,” *Results Phys.* **31**, 104909 (2021).

³⁶C. Yang, L. Mei, X. Wang, H. Deng, M. Hu, Z. Xu, B. Chen, Y. He, and R. Kan, “Simultaneous measurement of gas absorption and path length by employing the first harmonic phase angle method in wavelength modulation spectroscopy,” *Opt. Express* **28**, 3289–3297 (2020).

³⁷J. T. Dobler, F. Harrison, E. V. Browell, B. Lin, D. M. Gregor, S. Kooi, Y. Choi, and S. Ismail, “Atmospheric CO_2 column measurements with an airborne intensity-modulated continuous wave 1.57 μm fiber laser LIDAR,” *Appl. Opt.* **52**(12), 2874–2892 (2013).

³⁸C. T. Zheng, W. L. Ye, J. Q. Huang, T. S. Cao, M. Lv, J. M. Dang, and Y. D. Wang, “Performance improvement of a near-infrared CH_4 detection device using wavelet-denoising-assisted wavelength modulation technique,” *Sens. Actuators B* **190**, 249–258 (2014).

³⁹J. Xia, C. Feng, F. Zhu, S. Zhang, A. A. Kolomenskii, J. Dong, and A. A. Schuessler, “Real-time measurement of methane in a turbulent atmosphere over kilometer long paths with denoising methods,” *Measurement* **168**, 108467 (2021).

⁴⁰G. F. Zhu, H. Q. Zhu, C. H. Yang, and W. H. Gui, “Improved Savitzky-Golay filtering algorithm for measuring a pharmaceutical vial’s oxygen content based on wavelength modulation spectroscopy,” *J. Opt. Technol.* **84**(5), 355–359 (2017).

⁴¹L. Tian, J. Sun, S. Zhang, A. A. Kolomenskii, H. A. Schuessler, Z. Wang, J. Xia, J. Chang, and Z. Liu, “Near-infrared methane sensor with neural network filtering,” *Sens. Actuators B* **354**, 131207 (2022).

⁴²S. M. Qu, M. Wang, and N. Li, “Mid-infrared trace CH_4 detector based on TDLAS-WMS,” *Spectrum Spectrum Anal.* **36**(10), 3174–3178 (2016).

⁴³Y. B. Wei, T. T. Zhang, Y. F. Li, Y. J. Zhao, C. Wang, and T. Y. Liu, “High-resolution fiber methane sensor based on diode laser and its data processing,” *Proc. SPIE* **8192**, 906 (2011).

⁴⁴L. W. Zhang, Z. R. Zhang, and P. S. Sun, “A dual-gas sensor for simultaneous detection of methane and acetylene based on time-sharing scanning assisted wavelength modulation spectroscopy,” *Spectrochim. Acta, Part A* **239**, 118495 (2020).

⁴⁵W. K. Liang, Y. F. Bi, Q. Zhou, X. Z. Dong, and T. L. Lv, “Developing CH_4 detection limit at $\lambda = 1.654 \mu\text{m}$ by suppressing optical interference fringes in wavelength modulation spectroscopy,” *Sens. Actuators B* **255**, 2614–2620 (2018).

⁴⁶B. Wei, T. Y. Liu, and J. Hu, “A high sensitivity methane detector based on laser absorption spectrum,” in *18th International Conference on Optical Communications and Networks (ICOON)* (IEEE, 2019), pp. 1–3.

⁴⁷Y. Cao, N. P. Sanchez, W. Jiang, R. J. Griffin, F. Xie, L. C. Hughes, D. Zah, and F. K. Tittel, “Simultaneous atmospheric nitrous oxide, methane and water vapor detection with a single continuous wave quantum cascade laser,” *Opt. Express* **23**(3), 2121–2132 (2015).

⁴⁸M. Nikodem, K. Krzempek, G. Dudzik, and K. Abramski, “Hollow core fiber-assisted absorption spectroscopy of methane at 3.4 μm ,” *Opt. Express* **26**(17), 21843–21848 (2018).

⁴⁹K. Liu, L. Wang, T. Tan, and G. S. Wang, “Highly sensitive detection of methane by near-infrared laser absorption spectroscopy using a compact dense-pattern multipass cell,” *Sens. Actuators B* **220**, 1000–1005 (2015).

⁵⁰J. Chen, A. Hangauer, R. Strzoda, and M. C. Amann, “VCSEL-based calibration-free carbon monoxide sensor at 2.3 μm with in-line reference cell,” *Appl. Phys. B* **102**(2), 381–389 (2011).

⁵¹R. Y. Cui, L. Dong, H. P. Wu, S. Z. Li, L. Zhang, W. G. Ma, and W. B. Yin, “Highly sensitive and selective CO sensor using a 2.33 μm diode laser and wavelength modulation spectroscopy,” *Opt. Express* **26**(19), 24318–24328 (2018).

⁵²L. W. Zhang, Z. R. Zhang, and Q. J. Wang, “A sensitive carbon monoxide sensor for industrial process control based on laser absorption spectroscopy with a 2.3 μm distributed feedback laser,” *Opt. Lasers Eng.* **152**, 106984 (2022).

⁵³G. Ramin and F. M. Schmidt, “ICL-based TDLAS sensor for real-time breath gas analysis of carbon monoxide isotopes,” *Opt. Express* **25**(11), 12743–12752 (2017).

⁵⁴C. L. Li, Y. F. Wu, X. B. Qiu, J. Wei, and L. H. Deng, “Pressure-dependent detection of carbon monoxide employing wavelength modulation spectroscopy using a Herriott-type cell,” *Appl. Spectrosc.* **71**(5), 809–816 (2017).

⁵⁵N. Javis, Z. Qu, O. Werhahn, and E. Volker, “Interband cascade laser-based optical transfer standard for atmospheric carbon monoxide measurements,” *Appl. Opt.* **56**(11), E84–E93 (2017).

⁵⁶W. Wang and Z. Zhang, in *2018 International Symposium on Computer, Consumer and Control (IS3C)* (IEEE, 2018), p. 294.

⁵⁷A. Roy and A. L. Chakraborty, “QCL-Based open-path, single-pass measurement of ambient carbon monoxide using $R_{1f}/\Delta I_1$ WMS,” *IEEE Photonics Technol. Lett.* **33**(18), 982–985 (2021).

⁵⁸W. Y. Peng, R. Sur, C. L. Strand, R. M. Spearrin, J. B. Jeffries, and R. K. Hanson, “High-sensitivity *in situ* QCLAS-based ammonia concentration sensor for high-temperature applications,” *Appl. Phys. B* **122**(7), 1–12 (2016).

⁵⁹D. Stachowiak, P. Jaworski, P. Krzaczek, G. Maj, and M. Nikodem, “Laser-based monitoring of CH_4 , CO_2 , NH_3 , and H_2S in animal farming—System characterization and initial demonstration,” *Sensors* **18**(2), 529 (2018).

⁶⁰Q. B. Huang, X. M. Xu, C. J. Li, Y. P. Ding, C. Cao, L. Z. Yin, and J. F. Ding, “Self-calibration wavelength modulation spectroscopy for acetylene detection based on tunable diode laser absorption spectroscopy,” *Chin. Phys. B* **25**(11), 114202 (2016).

⁶¹M. L. Zou, Z. Yang, L. Q. Sun, and X. S. Ming, “Acetylene sensing system based on wavelength modulation spectroscopy using a triple-row circular multipass cell,” *Opt. Express* **28**(8), 11573–11582 (2020).

⁶²H. Y. Sun, Y. F. Ma, Y. He, S. D. Qiao, X. Yang, and F. K. Tittel, “Highly sensitive acetylene detection based on a compact multi-pass gas cell and optimized wavelength modulation technique,” *Infrared Phys. Technol.* **102**, 103012 (2019).

⁶³Q. X. He, C. T. Zheng, H. F. Liu, B. Li, Y. D. Wang, and F. K. Tittel, “Performance improvement of a near-infrared acetylene sensor system by reducing residual amplitude modulation,” *Laser Phys.* **27**(5), 055702 (2017).

⁶⁴R. Anirban, S. N. Kumar, C. Arup Lal, and U. Abhishek, “Measurement of atmospheric carbon dioxide and water vapor in built-up urban areas in the Gandhinagar-Ahmedabad region in India using a portable tunable diode laser spectroscopy system,” *Appl. Opt.* **56**(31), H57–H66 (2017).

⁶⁵P. Zhao, J. Tao, C. R. Yu, and Y. Li, *Research on the Trace Detection of Carbon Dioxide Gas and Modulation Parameter Optimization Based on the TDLAS Technology* (SPIE, 2014).

⁶⁶M. Q. Pi, C. T. Zheng, H. Zhao, Z. H. Peng, J. M. Lang, J. L. Ji, L. Liang, Y. Zhang, Y. Wang, and F. K. Tittel, “Mid-infrared $\text{CH}_3\text{g-on-MgF}_2$ waveguide gas

sensor based on wavelength modulation spectroscopy," *Opt. Lett.* **46**(19), 4797–4800 (2021).

⁶⁷Z. W. Liu, C. T. Zheng, C. Chen, Y. F. Li, H. T. Xie, Q. Ren, Y. D. Wang, and F. K. Tittel, "ICL-based mid-infrared carbon dioxide sensor system for deep-sea natural gas hydrate exploration," *Opt. Express* **27**(4), 5598–5609 (2019).

⁶⁸Y. F. Li, Z. W. Liu, T. Y. Zhang, C. T. Zheng, and Y. D. Wang, "Development and application of near infrared laser carbon dioxide gas sensor system," *Acta Opt. Sin.* **40**, 0514003 (2020).

⁶⁹C. G. Lou, C. R. Jing, X. Wang, Y. H. Chen, J. T. Zhang, K. Hou, J. Yao, and X. Liu, "Near-infrared tunable diode laser absorption spectroscopy-based determination of carbon dioxide in human exhaled breath," *Biomed. Opt. Express* **10**(11), 5486–5496 (2019).

⁷⁰M. Köhring, S. Huang, M. Jahjah, W. Jiang, W. Ren, U. Willer, C. Caneba, L. Yang, D. Nagrath, W. Schade, and F. K. Tittel, "QCL-based TDLAS sensor for detection of NO toward emission measurements from ovarian cancer cells," *Appl. Phys. B* **117**(1), 445–451 (2014).

⁷¹X. Chao, J. B. Jeffries, and R. K. Hanson, "Wavelength-modulation-spectroscopy for real-time, *in situ* NO detection in combustion gases with a 5.2 μm quantum-cascade laser," *Appl. Phys. B* **106**(4), 987–997 (2012).

⁷²X. T. Yang, W. Q. Xie, and Z. G. Yuan, "Research on the NO concentration of marine diesel emission by tunable diode laser absorption spectroscopy technique," *Optik* **127**, 3788–3791 (2016).

⁷³A. Fried, S. Sewell, B. Henry, B. P. Wert, T. Gilpin, and J. R. Drummond, "Tunable diode laser absorption spectrometer for ground-based measurements of formaldehyde," *J. Geophys. Res.: Atmos.* **102**(D5), 6253–6266, <https://doi.org/10.1029/96JD01580> (1997).

⁷⁴R. Wei, L. Q. Luo, and F. K. Tittel, "Sensitive detection of formaldehyde using an interband cascade laser near 3.6 μm ," *Sens. Actuators B* **221**, 1062–1068 (2015).

⁷⁵L. Dong, Y. Yu, C. Li, S. So, and F. K. Tittel, "Ppb-level formaldehyde detection using a CW room-temperature interband cascade laser and a miniature dense pattern multipass gas cell," *Opt. Express* **23**(15), 19821–19830 (2015).

⁷⁶L. S. Rothman, I. E. Gordon, Y. Babikov, A. Barbe, D. Chris Benner, P. F. Bernath, M. Birk, L. Bizzocchi, V. Boudon, L. R. Brown, A. Campargue, K. Chance, E. A. Cohen, L. H. Coudert, V. M. Devi, B. J. Drouin, A. Fayt, J. M. Flaud, R. R. Gamache, J. J. Harrison, J. M. Hartmann, C. Hill, J. T. Hodges, D. Jacquemart, A. Jolly, J. Lamouroux, R. J. Le Roy, G. Li, D. A. Long, O. M. Lyulin, C. J. Mackie, S. T. Massie, S. Mikhailenko, H. S. P. Mueller, O. V. Naumenko, A. V. Nikitin, J. Orphal, V. Perevalov, A. Perrin, E. R. Polovtseva, C. Richard, M. A. H. Smith, E. Starikova, K. Sung, S. Tashkun, J. Tennyson, G. C. Toon, V. G. Tyuterev, and G. Wagner, "The HITRAN 2012 molecular spectroscopic database," *J. Quant. Spectrosc. Radiat. Transf.* **130**, 4–50 (2013).

⁷⁷S. Maithani and M. Pradhan, "Cavity ring-down spectroscopy and its applications to environmental, chemical, and biomedical systems," *J. Chem. Sci.* **132**(1), 1–19 (2020).

⁷⁸D. Z. Anderson, J. C. Frisch, and C. S. Masser, "Mirror reflectometer based on optical cavity decay time," *Appl. Opt.* **23**(8), 1238–1245 (1984).

⁷⁹D. Romanini, A. A. Kachanov, N. Sadeghi, and F. Stoeckel, "CW cavity ring down spectroscopy," *Chem. Phys. Lett.* **264**(3–4), 316–322 (1997).

⁸⁰D. Gatti, T. Sala, R. Gotti, L. Cocola, L. Poletto, M. Prevedelli, P. Laporta, and M. Marangoni, "Comb-locked cavity ring-down spectrometer," *J. Chem. Phys.* **142**(7), 074201 (2015).

⁸¹L. E. McHale, A. Hecobian, and A. P. Yalin, "Open-path cavity ring-down spectroscopy for trace gas measurements in ambient air," *Opt. Express* **24**(5), 5523–5535 (2016).

⁸²S. Das, S. Pal, and M. Mitra, "Significance of exhaled breath test in clinical diagnosis: A special focus on the detection of diabetes mellitus," *J. Med. Biol. Eng.* **36**(5), 605–624 (2016).

⁸³S. Das and M. Pal, "Non-invasive monitoring of human health by exhaled breath analysis: A comprehensive review," *J. Electrochem. Soc.* **167**(3), 037562 (2020).

⁸⁴A. Szabó, V. Ruzsany, K. Unterkofler, Á. Mohácsi, E. Tuboly, M. Boros, G. Szabó, H. Hinterhuber, and A. Amann, "Exhaled methane concentration profiles during exercise on an ergometer," *J. Breath Res.* **9**(1), 016009 (2015).

⁸⁵R. Selvaraj, N. J. Vasa, S. M. Shiva Nagendra, and B. Mizaiko, "Advances in mid-infrared spectroscopy-based sensing techniques for exhaled breath diagnostics," *Molecules* **25**(9), 2227 (2020).

⁸⁶R. J. Basseri, B. Basseri, M. Pimentel, K. Chong, A. Youdim, K. Low, L. Hwang, E. Soffer, C. Chang, and R. Mathur, "Intestinal methane production in obese individuals is associated with a higher body mass index," *J. Gastroenterol. Hepatol.* **8**(1), 22–28 (2012).

⁸⁷J. H. Kim, E. Lin, and M. Pimentel, "Biomarkers of irritable bowel syndrome," *J. Neurogastroenterol. Motil.* **23**(1), 20 (2017).

⁸⁸K. W. Busch and M. A. Busch, *Cavity-Ringdown Spectroscopy: An Ultratrace-Absorption Measurement Technique* (ACS Publications, 1999).

⁸⁹S. Leon, *Linear Algebra with Applications, Featured Titles for Linear Algebra (Introductory) Series*, 5th ed. (Pearson, Boston, 2013), Chap. Orthogonality, p. 240.

⁹⁰A. Bicer, J. Bounds, F. Zhu, A. A. Kolomenskii, N. Kaya, E. Aluauee, M. Amani, and H. A. Schuessler, "Sensitive spectroscopic analysis of biomarkers in exhaled breath," *Int. J. Thermophys.* **39**(6), 1–11 (2018).

⁹¹A. Bicer, "Cavity ring-down spectroscopy of trace components in gas mixtures for breath analysis and environmental applications," Ph.D. dissertation (Texas A&M University, 2018).

⁹²G. Tusman, F. S. Sipmann, and S. H. Bohm, "Rationale of dead space measurement by volumetric capnography," *Anesth. Analg.* **114**, 866–874 (2012).

⁹³A. Rezaie, M. Buresi, A. Lembo, H. Lin, R. McCallum, S. Rao, M. Schmulson, M. Valdovinos, S. Zakko, and M. Pimentel, "Hydrogen and methane-based breath testing in gastrointestinal disorders: The North American consensus," *Am. J. Gastroenterol.* **112**(5), 775–784 (2017).

⁹⁴B. A. Paldus and C. C. Harb, "Cavity ringdown spectroscopy using mid-infrared quantum-cascade lasers," *Opt. Lett.* **25**(9), 666–668 (2000).

⁹⁵M. W. Todd, R. A. Provencal, T. G. Owano, B. A. Paldus, A. Kachanov, K. L. Vodopyanov, M. Hunter, S. L. Coy, J. I. Steinfeld, and J. T. Arnold, "Application of mid-infrared cavity-ringdown spectroscopy to trace explosives vapor detection using a broadly tunable (6–8 μm) optical parametric oscillator," *Appl. Phys. B: Lasers Opt.* **75**, 367–376 (2002).

⁹⁶D. A. Long, A. J. Fleisher, Q. Liu, and J. T. Hodges, "Ultra-sensitive cavity ring-down spectroscopy in the mid-infrared spectral region," *Opt. Lett.* **41**(7), 1612–1615 (2016).

⁹⁷R. Terabayashi, K. Saito, V. Sonnenschein, Y. Okuyama, T. Iguchi, M. Yamanaka, N. Nishizawa, K. Yoshida, S. Ninomiya, and H. Tomita, "Mid-infrared cavity ring-down spectroscopy using DFB quantum cascade laser with optical feedback for radiocarbon detection," *Jpn. J. Appl. Phys.* **59**, 092007 (2020).

⁹⁸A. Cygan, D. Lisak, S. Wójtewicz, J. Domyslawska, J. T. Hodges, R. S. Trawiński, and R. Ciuryło, "High-signal-to-noise-ratio laser technique for accurate measurements of spectral line parameters," *Phys. Rev. A* **85**, 022508 (2012).

⁹⁹D. A. Long, G.-W. Truong, R. D. van Zee, D. F. Plusquellic, and J. T. Hodges, "Frequency-agile, rapid scanning spectroscopy absorption sensitivity of $2 \times 10^{-12} \text{ cm}^{-1} \text{ Hz}^{-1/2}$ with a tunable diode laser," *Appl. Phys. B* **114**, 489–495 (2014).

¹⁰⁰J. Burkart, D. Romanini, and S. Kassi, "Optical feedback frequency stabilized cavity ring-down spectroscopy," *Opt. Lett.* **39**, 4695–4698 (2014).

¹⁰¹A. Maity, M. Pal, G. D. Banik, S. Maithani, and M. Pradhan, "Cavity ring-down spectroscopy using an EC-QCL operating at 7.5 μm for direct monitoring of methane isotopes in air," *Laser Phys. Lett.* **14**(11), 115701 (2017).

¹⁰²H. Fleurbaey, Z. D. Reed, E. M. Adkins, D. A. Long, and J. T. Hodges, "High accuracy spectroscopic parameters of the 1.27 μm band of O_2 measured with comb-referenced, cavity ring-down spectroscopy," *J. Quant. Spectrosc. Radiat. Transf.* **270**, 107684 (2021).

¹⁰³D. Lisak, D. Charczun, A. Nishiyama, T. Voumard, T. Wildi, G. Kowzan, V. Brasch, T. Herr, A. J. Fleisher, J. T. Hodges, R. Ciuryło, A. Cygan, and

- P. Masłowski, "Dual comb cavity ring down spectroscopy," *Sci. Rep.* **12**, 2377 (2022).
- ¹⁰⁴J. N. Eckstein, A. I. Ferguson, and T. W. Hänsch, "High-resolution two-photon spectroscopy with picosecond light," *Phys. Rev. Lett.* **40**(13), 847–850 (1978).
- ¹⁰⁵S. A. Diddams, D. J. Jones, J. Ye, S. T. Cundiff, J. L. Hall, J. K. Ranka, R. S. Windeler, R. Holzwarth, T. Udem, and T. W. Hänsch, "Direct link between microwave and optical frequencies with a 300 THz femtosecond laser comb," *Phys. Rev. Lett.* **84**(22), 5102–5105 (2000).
- ¹⁰⁶J. Reichert, M. Niering, R. Holzwarth, M. Weitz, Th. Udem, and T. W. Hänsch, "Phase coherent vacuum-ultraviolet to radio frequency comparison with a mode-locked laser," *Phys. Rev. Lett.* **84**(15), 3232–3235 (2000).
- ¹⁰⁷R. Holzwarth, Th. Udem, T. W. Hänsch, J. C. Knight, W. J. Wadsworth, and P. S. J. Russell, "Optical frequency synthesizer for precision spectroscopy," *Phys. Rev. Lett.* **85**(11), 2264–2267 (2000).
- ¹⁰⁸Th. Udem, R. Holzwarth, and T. W. Hänsch, "Optical frequency metrology," *Nature* **416**(6877), 233–237 (2002).
- ¹⁰⁹S. A. Diddams, K. Vahala, and T. Udem, "Optical frequency combs: Coherently uniting the electromagnetic spectrum," *Science* **369**(6501), 267 (2020).
- ¹¹⁰A. Parriaux, K. Hammani, and G. Millot, "Electro-optic frequency combs," *Adv. Opt. Photonics* **12**(1), 223 (2020).
- ¹¹¹A. Pasquazi, M. Peccianti, L. Razzari, D. J. Moss, S. Coen, M. Erkintalo, Y. K. Chembo, T. Hansson, S. Wabnitz, P. Del'Haye, X. Xue, A. M. Weiner, and R. Morandotti, "Micro-combs: A novel generation of optical sources," *Phys. Rep.* **729**, 1–81 (2018).
- ¹¹²M. G. Suh and K. J. Vahala, "Soliton microcomb range measurement," *Science* **359**(6378), 884–887 (2018).
- ¹¹³J. Riemensberger, A. Lukashchuk, M. Karpov, W. Weng, E. Lucas, J. Liu, and T. J. Kippenberg, "Massively parallel coherent laser ranging using a soliton microcomb," *Nature* **581**, 164–170 (2020).
- ¹¹⁴S. A. Diddams, Th. Udem, J. C. Bergquist, E. A. Curtis, R. E. Drullinger, L. Hollberg, W. M. Itano, W. D. Lee, C. W. Oates, K. R. Vogel, and D. J. Wineland, "An optical clock based on a single trapped $^{199}\text{Hg}^+$ ion," *Science* **293**(5531), 825–828 (2001).
- ¹¹⁵T. Udem, S. A. Diddams, K. R. Vogel, C. W. Oates, E. A. Curtis, W. D. Lee, W. M. Itano, R. E. Drullinger, J. C. Bergquist, and L. Hollberg, "Absolute frequency measurements of the Hg^+ and Ca optical clock transitions with a femtosecond laser," *Phys. Rev. Lett.* **86**(22), 4996–4999 (2001).
- ¹¹⁶N. Picqué and T. W. Hänsch, "Frequency comb spectroscopy," *Nat. Photonics* **13**(3), 146–157 (2019).
- ¹¹⁷T. Steinmetz, T. Wilken, C. Araujo-Hauck, R. Holzwarth, T. W. Hänsch, L. Pasquini, A. Manescau, S. D'Odorico, M. T. Murphy, T. Kentscher, W. Schmidt, and T. Udem, "Laser frequency combs for astronomical observations," *Science* **321**(5894), 1335–1337 (2008).
- ¹¹⁸P. Marin-Palomo, J. N. Kemal, M. Karpov, A. Kordts, J. Pfeifle, M. H. P. Pfeiffer, P. Trocha, S. Wolf, V. Brasch, M. H. Anderson, R. Rosenberger, K. Vijayan, W. Freude, T. J. Kippenberg, and C. Koos, "Microresonator-based solitons for massively parallel coherent optical communications," *Nature* **546**(7657), 274–279 (2017).
- ¹¹⁹I. Coddington, W. C. Swann, L. Nenadovic, and N. R. Newbury, "Rapid and precise absolute distance measurements at long range," *Nat. Photonics* **3**(6), 351–356 (2009).
- ¹²⁰F. Zhu, J. Xia, A. Bicer, J. Bounds, A. Kolomenskii, J. Strohaber, L. Johnson, M. Amani, and H. Schuessler, "Probing methane in air with a mid-infrared frequency comb source," *Appl. Opt.* **56**(22), 6311–6316 (2017).
- ¹²¹J. Mandon, G. Guelachvili, and N. Picqué, "Fourier transform spectroscopy with a laser frequency comb," *Nat. Photonics* **3**(2), 99–102 (2009).
- ¹²²G. B. Rieker, F. R. Giorgetta, W. C. Swann, J. Kofler, A. M. Zolot, L. C. Sinclair, E. Baumann, C. Cromer, G. Petron, C. Sweeney, P. P. Tans, I. Coddington, and N. R. Newbury, "Frequency-comb-based remote sensing of greenhouse gases over kilometer air paths," *Optica* **1**(5), 290–298 (2014).
- ¹²³K. C. Cossel, E. M. Waxman, F. R. Giorgetta, M. Cermak, I. R. Coddington, D. Hesselius, S. Ruben, W. C. Swann, G. Truong, G. B. Rieker, and N. R. Newbury, "Open-path dual-comb spectroscopy to an airborne retroreflector," *Optica* **4**(7), 724 (2017).
- ¹²⁴S. Coburn, C. B. Alden, R. Wright, K. Cossel, E. Baumann, G. W. Truong, F. Giorgetta, C. Sweeney, N. R. Newbury, K. Prasad, I. Coddington, and G. B. Rieker, "Regional trace-gas source attribution using a field-deployed dual frequency comb spectrometer," *Optica* **5**(4), 320–327 (2018).
- ¹²⁵G. Ycas, F. R. Giorgetta, K. C. Cossel, E. M. Waxman, E. Baumann, N. R. Newbury, and I. Coddington, "Mid-infrared dual-comb spectroscopy of volatile organic compounds across long open-air paths," *Optica* **6**(2), 165–168 (2019).
- ¹²⁶F. Zhu, H. Hundertmark, A. A. Kolomenskii, J. Strohaber, R. Holzwarth, and H. A. Schuessler, "High-power mid-infrared frequency comb source based on a femtosecond Er:fiber oscillator," *Opt. Lett.* **38**(13), 2360–2362 (2013).
- ¹²⁷M. J. Thorpe, K. D. Moll, R. J. Jones, B. Safdi, and J. Ye, "Broadband cavity ringdown spectroscopy for sensitive and rapid molecular detection," *Science* **311**(5767), 1595–1599 (2006).
- ¹²⁸A. Foltynowicz, T. Ban, P. Masłowski, F. Adler, and J. Ye, "Quantum-noise-limited optical frequency comb spectroscopy," *Phys. Rev. Lett.* **107**(23), 233002 (2011).
- ¹²⁹M. J. Thorpe, D. Balslev-Clausen, M. S. Kirchner, and J. Ye, "Cavity-enhanced optical frequency comb spectroscopy: Application to human breath analysis," *Opt. Express* **16**(4), 2387–2397 (2008).
- ¹³⁰G. Kowzan, K. F. Lee, M. Borkowski, P. Ablewski, S. Wójciewicz, K. Stec, D. Lisak, M. E. Fermann, R. S. Trawiński, and P. Masłowski, "VIPA spectrometer calibration and comb-cavity locking schemes comparison for sensitive and accurate frequency comb spectroscopy," *J. Phys.: Conf. Ser.* **810**, 012035 (2017).
- ¹³¹Q. Liang, Y. C. Chan, P. B. Changala, D. J. Nesbitt, J. Ye, and J. Toscano, "Ultrasensitive multispecies spectroscopic breath analysis for real-time health monitoring and diagnostics," *Proc. Natl. Acad. Sci. U.S.A.* **118**(40), e2105063118 (2021).
- ¹³²S. Schiller, "Spectrometry with frequency combs," *Opt. Lett.* **27**(9), 766 (2002).
- ¹³³F. Keilmann, C. Gohle, and R. Holzwarth, "Time-domain mid-infrared frequency comb spectrometry," *Opt. Lett.* **29**(13), 1542 (2004).
- ¹³⁴I. Coddington, W. Swann, and N. Newbury, "Coherent multiheterodyne spectroscopy using stabilized optical frequency combs," *Phys. Rev. Lett.* **100**(1), 013902 (2008).
- ¹³⁵P. Giaccari, J. D. Deschenes, P. Saucier, J. Genest, and P. Tremblay, "Active Fourier-transform spectroscopy combining the direct RF beating of two fiber-based mode-locked lasers with a novel referencing method," *Opt. Express* **16**(6), 4347–4365 (2008).
- ¹³⁶J. Roy, J. D. Deschenes, S. Potvin, and J. Genest, "Continuous real-time correction and averaging for frequency comb interferometry," *Opt. Express* **20**(20), 21932–21939 (2012).
- ¹³⁷T. Ideguchi, A. Poisson, G. Guelachvili, N. Picqué, and T. W. Hänsch, "Adaptive real-time dual-comb spectroscopy," *Nat. Commun.* **5**(1), 3375 (2014).
- ¹³⁸B. Lomsadze and S. T. Cundiff, "Frequency combs enable rapid and high-resolution multidimensional coherent spectroscopy," *Science* **357**(6358), 1389 (2017).
- ¹³⁹B. Lomsadze and S. T. Cundiff, "Frequency-comb based double-quantum two-dimensional spectrum identifies collective hyperfine resonances in atomic vapor induced by dipole-dipole interactions," *Phys. Rev. Lett.* **120**(23), 233401 (2018).
- ¹⁴⁰S. Mehravar, R. A. Norwood, N. Peyghambarian, and K. Kieu, "Real-time dual-comb spectroscopy with a free-running bidirectionally mode-locked fiber laser," *Appl. Phys. Lett.* **108**(23), 231104 (2016).
- ¹⁴¹A. E. Akosman and M. Y. Sander, "Dual comb generation from a mode-locked fiber laser with orthogonally polarized interlace pulses," *Opt. Express* **25**(16), 18592–18602 (2017).
- ¹⁴²J. Fellingner, A. S. Mayer, G. Winkler, W. Grosinger, G. Truong, S. Droste, C. Li, C. M. Heyl, I. Hartl, and O. H. Heckl, "Tunable dual-comb from an all-polarization-maintaining single-cavity dual-color Yb:fiber laser," *Opt. Express* **27**(20), 28062–28074 (2019).

- ¹⁴³M. J. Yu, Y. Okawachi, A. G. Griffith, N. Picqué, M. Lipson, and A. L. Gaeta, "Silicon-chip based mid-infrared dual-comb spectroscopy," *Nat. Commun.* **9**(1), 1869 (2018).
- ¹⁴⁴P. Trocha, M. Karpov, D. Ganin, M. H. P. Pfeiffer, A. Kordts, S. Wolf, J. Krockenberger, P. Marin-Palomo, C. Weimann, S. Randel, W. Freude, T. J. Kippenberg, and C. Koos, "Ultrafast optical ranging using microresonator soliton frequency combs," *Science* **359**(6378), 887–891 (2018).
- ¹⁴⁵B. Jerez, F. Walla, A. Betancur, P. Martín-Mateos, C. de Dios, and P. Acedo, "Electro-optic THz dual-comb architecture for high-resolution, absolute spectroscopy," *Opt. Lett.* **44**(2), 415–418 (2019).
- ¹⁴⁶X. Zhao, X. Qu, F. Zhang, Y. Zhao, and G. Tang, "Absolute distance measurement by multi-heterodyne interferometry using an electro-optic triple comb," *Opt. Lett.* **43**(4), 807–810 (2018).
- ¹⁴⁷A. M. Zolot, F. R. Giorgetta, E. Baumann, J. W. Nicholson, W. C. Swann, I. Coddington, and N. R. Newbury, "Direct-comb molecular spectroscopy with accurate, resolved comb teeth over 43 THz," *Opt. Lett.* **37**(4), 638–640 (2012).
- ¹⁴⁸Z. Chen, M. Yan, T. W. Hänsch, and N. Picqué, "A phase-stable dual-comb interferometer," *Nat. Commun.* **9**(1), 3035 (2018).
- ¹⁴⁹L. A. Sterczewski, A. Przewoka, W. Kaszub, and J. Sotor, "Computational Doppler-limited dual-comb spectroscopy with a free-running all-fiber laser," *APL Photonics* **4**(11), 116102 (2019).
- ¹⁵⁰Y. Nakajima, Y. Y. Hata, and K. Minoshima, "All polarization-maintaining polarization-multiplexed dual-comb fiber laser with a nonlinear amplifying loop mirror," *Opt. Express* **27**(10), 14648 (2019).
- ¹⁵¹K. J. Zhao, Y. Li, X. S. Xiao, and C. Yang, "Nonlinear multimode interference-based dual-color mode-locked fiber laser," *Opt. Lett.* **45**(7), 1655 (2020).
- ¹⁵²B. Bernhardt, A. Ozawa, P. Jacquet, M. Jacquy, Y. Kobayashi, T. Udem, R. Holzwarth, G. Guelachvili, T. W. Hänsch, and N. Picqué, "Cavity-enhanced dual-comb spectroscopy," *Nat. Photonics* **4**(1), 55–57 (2010).
- ¹⁵³A. J. Fleisher, D. A. Long, Z. D. Reed, J. T. Hodges, and D. F. Plusquellic, "Coherent cavity-enhanced dual-comb spectroscopy," *Opt. Express* **24**(10), 10424 (2016).
- ¹⁵⁴S. Boudreau, S. Levasseur, C. Perilla, S. Roy, and J. Genest, "Chemical detection with hyperspectral LiDAR using dual frequency combs," *Opt. Express* **21**(6), 7411–7418 (2013).
- ¹⁵⁵Z. Deng, Y. Liu, Z. Zhu, D. Luo, C. Gu, Z. Zuo, G. Xie, and W. Li, "Achieving precise spectral analysis and imaging simultaneously with a mode-resolved dual-comb interferometer," *Sensors* **21**(9), 3166 (2021).
- ¹⁵⁶T. R. S. Hayden, N. Malarich, D. Petrykowski, S. P. Nigam, J. D. Christopher, C. Lapointe, N. T. Wimer, P. E. Hamlington, and G. B. Rieker, "OH radical measurements in combustion environments using wavelength modulation spectroscopy and dual-frequency comb spectroscopy near 1491 nm," *Appl. Phys. B* **125**(12), 1–14 (2019).
- ¹⁵⁷T. Ideguchi, T. Nakamura, Y. Kobayashi, and K. Goda, "Kerr-lens mode-locked bidirectional dual-comb ring laser for broadband dual-comb spectroscopy," *Optica* **3**(7), 748–753 (2016).
- ¹⁵⁸A. Asahara, A. Nishiyama, S. Yoshida, K. I. Kondo, Y. Nakajima, and K. Minoshima, "Dual-comb spectroscopy for rapid characterization of complex optical properties of solids," *Opt. Lett.* **41**(21), 4971 (2016).
- ¹⁵⁹T. Ideguchi, S. Holzner, B. Bernhardt, G. Guelachvili, N. Picqué, and T. W. Hänsch, "Coherent Raman spectro-imaging with laser frequency combs," *Nature* **502**(7471), 355–358 (2013).
- ¹⁶⁰D. I. Herman, E. M. Waxman, G. Ycasa, F. R. Giorgetta, N. R. Newbury, and I. R. Coddington, "Real-time liquid-phase organic reaction monitoring with mid-infrared attenuated total reflectance dual frequency comb spectroscopy," *J. Mol. Spectrosc.* **356**, 39–45 (2019).
- ¹⁶¹A. Hipke, S. A. Meek, T. Ideguchi, T. W. Hänsch, and N. Picqué, "Broadband Doppler-limited two-photon and stepwise excitation spectroscopy with laser frequency combs," *Phys. Rev. A* **90**(1), 011805 (2014).
- ¹⁶²T. Ideguchi, B. Bernhardt, G. Guelachvili, T. W. Hänsch, and N. Picqué, "Raman induced Kerr-effect dual-comb spectroscopy," *Opt. Lett.* **37**(21), 4498–4500 (2012).
- ¹⁶³C. Gohle, B. Stein, A. Schliesser, T. Udem, and T. W. Hänsch, "Frequency comb vernier spectroscopy for broadband, high-resolution, high-sensitivity absorption and dispersion spectra," *Phys. Rev. Lett.* **99**, 263902 (2007).
- ¹⁶⁴L. Rutkowski and J. Morville, "Continuous vernier filtering of an optical frequency comb for broadband cavity-enhanced molecular spectroscopy," *J. Quant. Spectrosc. Radiat. Transf.* **187**, 204–214 (2017).
- ¹⁶⁵L. Rutkowski and J. Morville, "Broadband cavity-enhanced molecular spectra from vernier filtering of a complete frequency comb," *Opt. Lett.* **39**(23), 6664 (2014).
- ¹⁶⁶A. Khodabakhsh, V. Ramaiah-Badarla, L. Rutkowski, A. C. Johansson, K. F. Lee, J. Jiang, C. Mohr, M. E. Fermann, and A. Foltynowicz, "Fourier transform and vernier spectroscopy using an optical frequency comb at 3–5.4 μm ," *Opt. Lett.* **41**(11), 2541 (2016).
- ¹⁶⁷F. Zhu, J. Bounds, A. Bicer, J. Strohaber, A. A. Kolomenskii, C. Gohle, M. Amani, and H. A. Schuessler, "Near infrared frequency comb vernier spectrometer for broadband trace gas detection," *Opt. Express* **22**(19), 23026 (2014).
- ¹⁶⁸C. A. Alrahman, A. Khodabakhsh, F. M. Schmidt, Z. Qu, and A. Foltynowicz, "Cavity-enhanced optical frequency comb spectroscopy of high-temperature H_2O in a flame," *Opt. Express* **22**(11), 13889 (2014).
- ¹⁶⁹K. C. Cossel, F. Adler, K. A. Bertness, M. J. Thorpe, J. Feng, M. W. Raynor, and J. Ye, "Analysis of trace impurities in semiconductor gas via cavity-enhanced direct frequency comb spectroscopy," *Appl. Phys. B* **100**, 917–924 (2010).
- ¹⁷⁰N. B. Hébert, V. Michaud-Belleau, S. Magnan-Saucier, J. Deschênes, and J. Genest, "Dual-comb spectroscopy with a phase-modulated probe comb for sub-MHz spectral sampling," *Opt. Lett.* **41**(10), 2282–2285 (2016).
- ¹⁷¹Y. D. Hsieh, Y. Iyonaga, Y. Sakaguchi, S. Yokoyama, H. Inaba, K. Minoshima, F. Hindle, T. Araki, and T. Yasui, "Spectrally interleaved comb-mode-resolved spectroscopy using swept dual terahertz combs," *Sci. Rep.* **4**(1), 3816 (2015).
- ¹⁷²T. Yasui, Y. Iyonaga, Y. D. Hsieh, Y. Sakaguchi, F. Hindle, S. Yokoyama, T. Araki, and M. Hashimoto, "Super-resolution discrete Fourier transform spectroscopy beyond time-window size limitation using precisely periodic pulsed radiation," *Optica* **2**(5), 460–467 (2015).
- ¹⁷³N. R. Newbury, I. Coddington, and W. Swann, "Sensitivity of coherent dual-comb spectroscopy," *Opt. Express* **18**(8), 7929 (2010).
- ¹⁷⁴F. Zhu, A. Bicer, R. Askar, J. Bounds, A. A. Kolomenskii, V. Kelessides, M. Amani, and H. A. Schuessler, "Mid-infrared dual frequency comb spectroscopy based on fiber lasers for the detection of methane in ambient air," *Laser Phys. Lett.* **12**(9), 095701 (2015).
- ¹⁷⁵G. Porat, C. M. Heyl, S. B. Schoun, C. Benko, N. Dörre, K. L. Corwin, and J. Ye, "Phase-matched extreme-ultraviolet frequency-comb generation," *Nat. Photonics* **12**(7), 387–391 (2018).
- ¹⁷⁶T. Yasui, M. Nose, A. Ihara, K. Kawamoto, S. Yokoyama, H. Inaba, K. Minoshima, and T. Araki, "Fiber-based hybrid terahertz spectrometer using dual fiber comb," *Opt. Lett.* **35**(10), 1689 (2010).
- ¹⁷⁷C. Liu, J. Guo, L. Yu, J. Li, M. Zhang, H. Li, Y. Shi, and D. Dai, "Silicon/2D-material photodetectors: From near infrared to mid-infrared," *Light Sci. Appl.* **10**(1), 123 (2021).
- ¹⁷⁸F. Zhu, T. Mohamed, J. Strohaber, A. A. Kolomenskii, Th. Udem, and H. A. Schuessler, "Real-time dual frequency comb spectroscopy in the near infrared," *Appl. Phys. Lett.* **102**(12), 121116 (2013).
- ¹⁷⁹R. Gautam, S. Vanga, F. Ariese, and S. Umamathy, "Review of multidimensional data processing approaches for Raman and infrared spectroscopy," *EPJ Tech. Instrum.* **2**, 8 (2015).